

Soil moisture and streamflow deficit anomaly index: An approach to quantify drought hazards by combining deficit and anomaly

Eklavya Popat¹, Petra Döll^{1,2}

¹Institute of Physical Geography, Goethe University Frankfurt, Germany

²Senckenberg Leibniz Biodiversity and Climate Research Centre Frankfurt (S**b**B**i**K**k**-F), Frankfurt, Germany

Correspondence to: Eklavya Popat (popat@em.uni-frankfurt.de)

Abstract

Drought is understood as both a lack of water (i.e., a deficit as compared to ~~some requirement~~demand) and a temporal anomaly in the condition of one or more components of the hydrological cycle. Most drought indices, however, only consider the anomaly aspect, i.e., how unusual the condition is. In this paper, we present two drought hazard indices that reflect both the deficit and anomaly aspects. The soil moisture deficit anomaly index, SMDAI, is based on the drought severity index, DSI, but is computed in a more straightforward way that does not require the definition of a mapping function. We propose a new indicator of drought hazard for water supply from rivers, the streamflow deficit anomaly index, QDAI, which takes into account the surface water demand of humans and freshwater biota. Both indices are computed and analyzed at the global scale, with a spatial resolution of roughly 50 km, for the period 1981-2010, using monthly time series of variables computed by the global water resources and the model WaterGAP2.2d. We found that the SMDAI and QDAI values are broadly similar to values of purely anomaly-based indices. However, the deficit anomaly indices provide more differentiated spatial and temporal patterns that help to distinguish the degree and nature of the actual drought hazard to vegetation health or the water supply. QDAI can be made relevant for stakeholders with different perceptions about the importance of ecosystem protection, by adapting the approach for computing the amount of water that is required to remain in the river for the well-being of the river ecosystem. Both deficit anomaly indices are well suited for inclusion in local or global drought risk studies.

Keywords: drought index, anomaly, soil moisture deficit, streamflow deficit, water abstraction

1 Introduction

According to the Australian Bureau of Meteorology, “drought is a prolonged, abnormally dry period when the amount of available water is insufficient to meet our normal use (BoM, 2018)”. This definition describes drought as both an anomaly (“less water than normal”) and a deficit (“less water than required”), reflecting general non-expert notions of drought. However, most experts define drought only as an anomaly, for example, as “a lack of water compared to normal conditions which can occur in different components of the hydrological cycle” (Van Loon et al., 2016, p.3633). Assuming that humans

Formatted: Indent: First line: 1.27 cm

Formatted: Indent: First line: 1.27 cm

and other biota are accustomed to seasonal variations of water availability in the form of precipitation, soil moisture, streamflow, or groundwater storage, droughts are mostly defined by the deviation of a water quantity at a specific point in time (e.g., precipitation in May 2005) from its long-term mean or median (e.g., of all May precipitation values during the reference period 1981-2010). It is further assumed for most drought hazard indicators that humans and other biota are used to interannual variability. Therefore, drought is not defined by a percentage deviation but rather by using percentiles (e.g., precipitation in May 2005 is less than the 10th percentile of all May precipitation values during the reference period) or by standardized drought indicators where the anomaly is divided by the standard deviation. **Anomaly-based drought indicators that indicate “less water than normal”** include the Standardized Precipitation Index (SPI) (McKee et al., 1993), the Standardized Precipitation Evapotranspiration Index (SPEI) (Vicente-Serrano et al., 2010; Bergez et al., 2013), the China Z index (CZI) (Wu et al., 2001) and, for streamflow drought, the Standardized Streamflow Index (~~SSFI~~) (Modarres, 2007) and the percentile-based low-flow index by Cammalleri et al. (2017) can be used.

Some researchers have quantified drought by only considering the deficit aspect of drought, i.e., by computing the difference between an optimal water quantity and the actual quantity (“less water than required”). **Deficit-based indicators have only been derived for assessing drought risk for vegetation, as optimal water quantities can be defined by either the field capacity of the soil (Sridhar et al., 2008) or potential evapotranspiration. For the latter, the deficit is computed either as the difference between potential evapotranspiration and precipitation (Hogg et al., 2013) (Hogg et al., 2013) or between potential and actual evapotranspiration. Examples of deficit-based indicators include the Soil Moisture Deficit Index (SMDI) as well as the Evapotranspiration Deficit Index (ETDI) from Narasimhan and Srinivasan (2005) and the Soil Water Storage (SWS) from British Columbia Ministry of Agriculture (2015).** A drawback of these deficit-based drought hazard indicators is that they indicate strong drought events in arid and (semi)arid regions, even though the vegetation in these regions is adapted to generally lower soil moisture (Cammalleri et al., 2016). **Deficit-based indicators cannot be meaningfully derived for the variable precipitation only as the definition of an optimal precipitation amount depends on the user of the precipitation water. It is, however, conceptually meaningful to determine deficits for human water supply based on the variable streamflow, defining the deficit as the difference between the demand for water from the river and the actual streamflow.** To the best of our knowledge, streamflow drought has not, as yet, been characterized by a deficit-based drought indicator.

Two notable attempts in identifying and bringing together both the anomaly and deficit aspects are the Palmer Drought Severity Index (PDSI) (Palmer, 1965) and the Drought Severity Index (DSI) (Cammalleri et al., 2016). PDSI is a standardized index developed to quantify the cumulative deficit of moisture supply in the form of precipitation as compared to demand in the form of potential evapotranspiration; it indicates meteorological drought, has been extensively used in the USA (Heim, 2002) and its strengths and weaknesses have been investigated (Dai et al., 2004). DSI indicates soil moisture drought by combining the soil moisture deficit (as compared to the situation in which plant evapotranspiration is not constrained by soil moisture availability) and the anomaly of the deficit, thus indicating rare events in which plants suffer from water stress. An anomaly-based soil moisture drought may, however, be unsuitable for indicating a drought hazard for vegetation as, in areas with high soil moisture in most years, the low interannual variability and, thus, the standard deviation, would indicate a strong

Field Code Changed

Field Code Changed

Field Code Changed

Field Code Changed

Field Code Changed

Field Code Changed

Field Code Changed

Field Code Changed

Field Code Changed

Field Code Changed

Field Code Changed

Field Code Changed

Field Code Changed

drought hazard in years with unusually low soil moisture values that are, nevertheless, still close to the optimal values and do not cause any water stress for the plants (Cammalleri et al., 2016).

Field Code Changed

Similar to the demand for soil water by plants, humans have a demand for water from rivers in situations where they rely on river water for their water supply. About ~~75~~^{three-quarters}% of global water withdrawals for irrigation, cooling of thermal power plants, manufacturing and domestic use, ~~totaling~~^{totaling} about 3700 km³/a in the first decade of this century, are sourced from surface water (Döll et al., 2014). Globally, irrigation is the largest water demand sector, accounting for ~~more~~^{than} 60% of total surface water withdrawals (Müller Schmied et al., 2020; Döll et al., 2014). To date, however, streamflow drought indicators only describe the anomaly of streamflow but do not indicate whether there is enough water in the river to meet water demand. Thus, to assess the risk of drought for human water supply from rivers, an indicator that combines the anomaly of streamflow conditions with a deficit, with respect to water demand, is desirable. In this way, the locations and times where ~~the~~ human water supply is at risk can be identified.

Field Code Changed

Field Code Changed

Differing from anomaly-based streamflow drought indicators, a combined analysis of streamflow anomaly and deficit requires time series information of both streamflow and water demand. This information is available from global water resources and uses models such as WaterGAP with a spatial resolution of 0.5° (55 km by 55 km at the equator) and a monthly temporal resolution (Alcamo et al., 2003; Müller Schmied et al., 2020). Up to the present time, macro-scale drought risk assessments have included the demand for water as vulnerability indicators by using a country's average water withdrawal to water availability ratio (e.g., Meza et al., 2020).

Field Code Changed

Field Code Changed

In this study, we introduce ~~and relate~~ two drought hazard indicators that combine both the deficit and anomaly aspects: one for soil moisture drought and the other for streamflow drought. In the soil moisture deficit anomaly index (SMDAI), the deficit is calculated as the difference between the soil moisture at field capacity (that which should allow optimal, non-water-limited plant growth) and the actual soil moisture. The SMDAI slightly modifies and simplifies the DSI introduced by Cammalleri et al. (2016). Another difference from Cammalleri et al. (2016) is that the SMDAI is computed globally, using the output of WaterGAP, rather than just for Europe. The streamflow deficit anomaly index QDAI is, to our knowledge, the first-ever streamflow drought indicator that combines both the anomaly and deficit aspects of streamflow drought. In the case of QDAI, the deficit is computed by comparing actual streamflow to the combined human and environmental surface water demand per grid cell. QDAI focuses on determining the drought hazard for the water supply for humans, including domestic, industrial, and irrigation water demand. QDAI is constructed similarly to SMDAI and computed globally using WaterGAP. Whether QDAI should be called a drought hazard indicator, or a combined drought hazard and vulnerability indicator, is up for discussion. However, for global-scale drought risk assessments, gridded QDAI values can be meaningfully combined with country-scale vulnerability indicators of, for example, coping capacity.

Field Code Changed

Field Code Changed

In Section 2, we describe (a) the methods for calculating SMDAI and QDAI and (b) how ~~water demand~~, streamflow, surface water use, and soil moisture are computed by WaterGAP 2.2d (Müller Schmied et al., 2020). In section 3, spatial and temporal patterns of SMDAI and QDAI are presented. In Section 4, we analyze the components of SMDAI and QDAI, compare

Field Code Changed

SMDAI to DSI, compare QDAI to a standardized streamflow indicator (*SSF/ISSFI*) and discuss the limitations of the study. Finally, we draw conclusions in Section 5.

2. Methods and data

2.1 Global-scale simulation of soil moisture, soil water capacity, streamflow and human water ~~withdrawal~~abstraction

In this study, we use the output of the latest version of the global hydrological and water use model WaterGAP 2.2d (Müller Schmied et al., 2020). WaterGAP consists of ~~two-three~~ major ~~modules~~components: the water use models ~~for five different sectors, the linking model GSWUSE~~ and the global hydrological model (WGHM). ~~The water use models compute water use in the five sectors household, manufacturing, cooling of thermal power plants, livestock and irrigation. Household and manufacturing water use is computed based on national statistics (Flörke et al., 2013) (Flörke et al., 2013). The amount of water required for cooling of thermal power plants is calculated based on the location, type, and size of power plants and the annual time series of thermal electricity production (Flörke et al., 2013) (Flörke et al., 2013). The globally small amount of livestock water use is determined from the number of livestock and livestock-specific water use values (Alcamo et al., 2003). Irrigation water use is computed based on information on the irrigated area and climate for each grid cell. The irrigation model first computes cell-specific cropping patterns and growing periods and then irrigation consumptive water use, distinguishing only rice and non-rice crops (Döll and Siebert, 2002). The irrigated areas are changing over time (Siebert et al., 2015) (Siebert et al., 2015).~~

~~The water use models do not take into account the source of the sectoral water abstractions. This is done by The submodel GWSWUSE, which distinguishes water use from groundwater and surface water sources and computes monthly time series of 0.5° grid-cell values of human water abstractions from 1) surface water bodies (river, lakes, and man-made reservoirs) and 2) groundwater, for each of the five sectors, as well as the respective net abstractions from both sources (Döll et al., 2012). A comparison of simulated annual sectoral water abstractions per country to independent values from the AQUASTAT database of FAO showed a rather high similarity between the two data sets (Müller Schmied et al., 2020).~~

Taking into account the net abstractions, ~~i.e. the difference between water abstractions and return flows~~, WGHM simulates, ~~with a spatial resolution of 0.5° by 0.5° (55 km by 55 km at the equator)~~ and a daily time step, the most relevant hydrological processes occurring on the continents and computes water flows such as actual evapotranspiration, runoff, groundwater recharge and streamflow, as well as the amount of water stored in diverse compartments such as the soil and the groundwater for all land areas, excluding Antarctica (Müller Schmied et al., 2014; Döll et al., 2003; Alcamo et al., 2003).

The soil is represented as one water storage compartment that is characterized by 1) soil water capacity (S_{max} - S_{min}), which is computed as the product of land cover, specific rooting depth, and soil water capacity in the upper meter and 2) soil texture, which affects groundwater recharge (Müller Schmied et al., 2014). The temporal development of soil moisture (*SS*) is computed from the balance of inflows (precipitation and snowmelt minus interception by the canopy) and outflows (actual evapotranspiration and total runoff from the land). Total runoff from the land fraction of the grid cell is then partitioned into

Field Code Changed

Formatted: Font: (Default) Times New Roman, 10 pt, English (United Kingdom)

Formatted: Font: (Default) Times New Roman, 10 pt, English (United Kingdom)

Formatted: Font: (Default) Times New Roman, 10 pt, English (United Kingdom)

Formatted: Font: (Default) Times New Roman, 10 pt, English (United Kingdom)

Field Code Changed

Formatted: Font: (Default) Times New Roman, English (United Kingdom)

Formatted: Font: (Default) Times New Roman, English (United Kingdom)

Field Code Changed

Formatted: Font: (Default) Times New Roman, English (United Kingdom)

Formatted: Font: (Default) Times New Roman, English (United Kingdom)

Formatted: Font: (Default) Times New Roman, English (United Kingdom)

Formatted: Font: (Default) Times New Roman, English (United Kingdom)

Formatted: Font: (Default) Times New Roman, English (United Kingdom)

Formatted: Font: (Default) Times New Roman, English (United Kingdom)

Field Code Changed

Field Code Changed

Field Code Changed

Field Code Changed

the fast surface and subsurface runoff and the diffuse groundwater recharge. Both components are subject to so-called fractional routing to the various other storages within the 0.5° grid cell, which include the groundwater as well as lakes, wetlands, man-made reservoirs, and rivers (Döll et al., 2014). Streamflow (Q_{ant}) in each grid cell depends on the runoff generated within the cell, inflow from upstream grid cells as well as human water abstractions and takes into account the impact of man-made reservoirs.

WGHM is calibrated to match long-term annual observed streamflows at the outlets of 1319 drainage basins that cover ~54 % of the global drainage area, following the calibration principles provided by Müller Schmied et al. (2014), Hunger and Döll (2008), and Döll et al. (2003). In validation studies against time series of observed streamflows, WaterGAP has been repeatedly shown to be among the best-performing global hydrological models (Zaherpour et al., 2019; Zaherpour et al., 2018; Veldkamp et al., 2018). Nevertheless, there can be significant mismatches between the observed and simulated seasonality and interannual variability.

This study uses simulated data of 30-years (1981 – 2010) monthly time series of WaterGAP gridded (0.5° x 0.5°) output of 67420 land grid cells covering all land areas of the globe except Greenland and Antarctica, for 1) soil moisture (S) [mm], 2) streamflow (Q_{ant}) [$\text{km}^3 \text{ month}^{-1}$], 3) streamflow under naturalized condition (Q_{nat}) [$\text{km}^3 \text{ month}^{-1}$], assuming there are no human water abstraction or man-made reservoirs, and 4) total surface water abstractions (WU_{sw}) [$\text{km}^3 \text{ month}^{-1}$]. In addition, the consistent dataset of soil water capacity (S_{max}) [mm] is utilized.

2.2 Computation of deficit and anomaly components of the soil moisture deficit anomaly index SMDAI

2.2.1 Deficit

Soil moisture deficit (d_{soil}) refers to the lack of water in the root zone for plants as compared to optimal growing conditions assumed to occur at soil water capacity (demand for water). d_{soil} is calculated as

$$d_{soil} = \frac{S_{max} - S}{S_{max}} \quad (1)$$

where S_{max} [mm] is the amount of water stored in the soil between field capacity and wilting point within the plant's root zone, S [mm] is the actual amount of soil water. d_{soil} ranges from 0 (no deficit/stress) to 1 (extreme deficit/stress).

2.2.2 Anomaly

Assuming that vegetation is used to seasonal variations of soil moisture, the anomaly of monthly soil moisture is determined separately for each calendar month. Interannual variability of both monthly soil moisture and monthly soil moisture deficit can be used to examine the occurrence frequency of soil moisture droughts and identify the normal state of the system.

Field Code Changed

Field Code Changed

Field Code Changed

Field Code Changed

Field Code Changed

Field Code Changed

Field Code Changed

Field Code Changed

Formatted: Font: 10 pt

Formatted Table

Formatted: Font: 10 pt

Field Code Changed

Formatted: Font: 10 pt

Formatted: Font: 10 pt

The unusualness of drought, compared to the normal state for a specific site and calendar month, is commonly quantified using In case of standardized drought indicators such as the SPI, the standard z-score. In general a so-called, the z-score is computed separately for each calendar month (here using, for example, 30 monthly soil moisture deficits in the 30 January months during the period 1981-2010), by standardizing the variable using the calendar month mean and standard deviation after translating the cumulative distribution function that optimally fits the distribution of monthly values to a normal distribution (McKee et al., 1993). Thus, computation of the z-score assumes that the vegetation is adapted to both seasonal and interannual variability. Following Cammalleri et al. (2016), in this study, we express the anomaly aspect of drought not by the z-score but by deriving a so-called drought probability index (p) that can be combined with the deficit indicator to a deficit-anomaly drought hazard index.

Computation of p also starts with identifying the probability of exceedance of a certain soil moisture deficit FF. Sheffield et al. (2004) found that long-term time series of soil moisture data per calendar month are best represented by the beta distribution function. The probability-density function f and cumulative density function F of the beta distribution function can be expressed as

$$F(d_{soil}; a, b) = \frac{B(d_{soil}; a, b)}{B(a, b)}$$

$$f(d_{soil}; a, b) = \frac{1}{B(a, b)} d_{soil}^{(a-1)} (1 - d_{soil})^{(b-1)} \quad (2)$$

$$F(d_{soil}; a, b) = \frac{B(d_{soil}; a, b)}{B(a, b)} \quad (3)$$

where $a, b \geq 0$ are the shape parameters, $B(a, b)$ is the beta function and $B(d_{soil}; a, b)$ is the incomplete beta function. In this form, the b supports the range of $d_{soil} \in [0, 1]$.

In this study, we could confirm the assumption made by Cammalleri et al. (2016) that the beta distribution function represents satisfactorily the distribution of d_{soil} , which is the same as that of the soil moisture itself. The beta cumulative distribution function was fitted to d_{soil} values for each calendar month and grid cell (i.e., for each grid cell, twelve beta functions are fitted corresponding to the twelve calendar months).

Following Cammalleri et al. (2016), the next step was to derive from FF a drought probability index (p_{soil}) that translates the probability that a certain soil water deficit status is drier than usual into the range [0, 1]. As suggested by Agnew (2000), a z-score of -0.84, which corresponds to a return period of 5 years and a $F(d_{soil})$ of 0.8, was assumed to be the threshold for drought (Table 1), for which $p_{soil} = 0$. Then, the drought probability index is calculated as

$$p_{soil} = \frac{F(d_{soil}) - 0.8}{1 - 0.8}$$

Field Code Changed

Field Code Changed

Formatted: Font: 10 pt

Field Code Changed

Formatted: Font: 10 pt

Formatted: Font: 10 pt

Formatted: Space Before: 6 pt, After: 6 pt

Formatted: Indent: First line: 0 cm

Field Code Changed

Formatted: Font: 10 pt

Field Code Changed

Formatted: Font: 10 pt

Formatted: Font: 10 pt

185
$$p_{soil} = \frac{F(d_{soil}) - 0.6}{1 - 0.6} \quad (4)$$

where $F(d_{soil})$ is the beta cumulative distribution function fitted to d_{soil} . If the beta cumulative distribution function is fitted to S , then $(1-F(S))$ should be used instead of $F(d_{soil})$.

190 Cammalleri et al. (2016) calculated p_{soil} using the mode instead of median as the reference for the normal status of d_{soil} . The computation of p_{soil} from $F(d_{soil})$ was carried out ~~done~~ in two steps. First, for d_{soil} values that are greater than or equal to the mode, a new standardized cumulative distribution function $F_{F^*}(d_{soil})$ is computed (Eq. 3 in Cammalleri et al., 2016). Subsequently, mapping of $F_{F^*}(d_{soil})$ values ranging from 0.6 to 1 are mapped onto the p_{soil} range of [0, 1], an by an exponential function (Eq. 4 in Cammalleri et al., 2016) was employed. This exponential function that was developed following considerations to subjectively fit subjectively, —fitted to subjectively—defined pairs of $F_{F^*}(d_{soil})$ and p_{soil} (Table 1 in Cammalleri et al., 2016) (Eq. 4 in Cammalleri et al., 2016). In this study, we have simplified the more unnecessarily complex approach of Cammalleri et al. (2016) by relying directly on $F(d_{soil})$ for mapping $F(d_{soil})$ onto p_{soil} according to Eq. 34 (Figure S1). In our opinion, there is no added value in defining an arbitrary exponential mapping function for deriving an indicator for the probability of a drought occurrence (p_{soil}). Furthermore, like most other drought researchers, we prefer the median to the mode, as among 30 deficit values, which are rational numbers, there is no true mode, i.e., no value that occurs most often. The relation between the anomaly component (p) of SMDAI (i.e., p_{soil}) to the non-exceedance probability of the soil moisture deficit ($F(d_{soil})$) and the pertaining return periods, z-scores, and class names, according to Agnew (2000) as well as the anomaly component (p) of DSI (p_{DSI}) is are presented in Table 1. A comparison of p_{soil} to p_{DSI} values as a function of $F(d_{soil})$ ($F(d_{soil})$) —as presented in Table 1 is shown in Figure S1 and the slight differences between p_{soil} and p_{DSI} as well as DSI and SMDAI, as well as DSI and SMDAI, computed with WaterGAP output for August 2003 at the global scale is are presented in Figure S2. For the period 1981-2010, SMDAI is, averaged over all grid cells, Also, a difference of 0.05 (on average per grid cell) larger is observed between SMDAI and than DSI values for the period of 1981–2010.

210 Furthermore, like most other drought researchers, we prefer the median to the mode, as among 30 deficit values, which are rational numbers, there is no true mode, i.e., no value that occurs most often. Table 1 shows the relationship of the anomaly component (p) of SMDAI (i.e., p_{soil}) to the non-exceedance probability of the soil moisture deficit ($F(d_{soil})$) and the pertaining return periods, z-scores and class names, according to Agnew (2000) as well as the p -values by Cammalleri et al. (2016) (p_{DSI}). Figure S2 shows, for the example of August 2003, that there are only slight differences between the values of p_{DSI} and p and of DSI and SMDAI, if they are all computed using WaterGAP output.

215

Field Code Changed

Field Code Changed

Formatted: English (United States)

Field Code Changed

Field Code Changed

Formatted: English (United States)

Formatted: English (United States)

220
225
230

Table 1. Relationship of the anomaly component p of SMDAI and QDAI to the non-exceedance probability of the soil moisture deficit ($F(d_{soil})$) or of streamflow ($F(Q)$), the pertaining return periods, z-scores and class names according to Agnew (2000) as well as the p-values by Cammalleri et al. (2016) to compute DSI. The class name refers to the drought conditions with z-score values that are larger than those listed in the z-score column. The equiprobability transformation technique, first suggested by Abramowitz and Stegun (1965) and utilized in Kumar et al. (2009) for calculation of the Standardized Precipitation Index (SPI), is used to back-calculate F values from the z-score values.

$F(d_{soil})/ F(Q)$	Return period (yrs)	z-score	Drought class name	p_DSI	P_{soil}/P_Q
0.8	5	-0.84	Normal	0	0
0.843	6.4	-1.00	Mild	0.04	0.21
0.87	7.7	-1.12	Moderate	0.10	0.35
0.9	10	-1.28	Moderate	0.26	0.50
0.933	15	-1.50	Moderate	0.54	0.68
0.95	20	-1.64	Severe	0.72	0.75
0.97	33.3	-1.88	Severe	0.89	0.85
0.9775	40	-2.00	Severe	0.93	0.88
0.99	99	-2.33	Extreme	0.99	0.95
0.995	200	-2.57	Extreme	0.997	0.97
0.998	500	-2.88	Extreme	0.999	0.99
1	--	~ -4.00	Extreme	~ 1	~ 1

2.3 Computation of deficit and anomaly components of the streamflow deficit anomaly index QDAI

2.3.1 Deficit

Similar to the soil moisture deficit, the streamflow deficit (d_Q) is calculated as the demand for water minus the supply divided by demand. It refers to the amount of streamflow that is lacking to satisfy the surface water demand of both humans and the river ecosystem. d_Q is computed as

$$d_Q = \frac{(WU_{sw} + EFR) - Q_{ant}}{WU_{sw} + EFR} \quad (4)$$

$$d_Q = \frac{(WU_{sw} + EFR) - Q_{ant}}{WU_{sw} + EFR} \quad (5)$$

where WU_{sw} [$\text{km}^3 \text{ month}^{-1}$] is water abstraction from surface water bodies, derived as the sum of water abstractions for irrigation, livestock, cooling of thermal power plants, manufacturing and household use. Q_{ant} [$\text{km}^3 \text{ month}^{-1}$] is the streamflow

- Field Code Changed
- Field Code Changed
- Field Code Changed
- Field Code Changed
- Formatted: Keep with next, Keep lines together
- Formatted: Font color: Text 1
- Formatted: Right, Keep with next, Keep lines together
- Formatted Table
- Formatted: Right, Keep with next, Keep lines together
- Formatted: Right, Keep with next, Keep lines together
- Formatted: Right, Keep with next, Keep lines together
- Formatted: Right, Keep with next, Keep lines together
- Formatted: Right, Keep with next, Keep lines together
- Formatted: Right, Keep with next, Keep lines together
- Formatted: Right, Keep with next, Keep lines together
- Formatted: Right, Keep with next, Keep lines together
- Formatted: Right, Keep with next, Keep lines together

Formatted: Indent: First line: 1.27 cm

Formatted: Font: 10 pt

Field Code Changed

Formatted: Font: 10 pt

Formatted: Font: 10 pt

Formatted: Indent: First line: 0 cm

and EFR [km³ month⁻¹] is the environmental flow requirement, i.e., the surface water demand of the river ecosystem. Following Richter et al. (2012), EFR is calculated for each calendar month as a function of mean monthly streamflow under the naturalized condition ($\overline{Q_{nat}}$), with

$$EFR = 0.8 \cdot \overline{Q_{nat}} \quad (5)$$

$$EFR = 0.8 \cdot \overline{Q_{nat}} \quad (6)$$

assuming that 80% of the natural mean monthly streamflow that would have occurred in the river without human water use and man-made reservoirs needs to remain in the river for the well-being of the river ecosystem. Differing from S_{max} , which represents the vegetation demand for soil water, the streamflow demand is temporally variable. d_Q is, like d_{soil} , in the range of 0 (no deficit/stress) to 1 (extreme deficit/stress); if d_Q is less than 0 or WU_{sw} equals 0, then d_Q is set to 0. To explore how assumptions about EFR and, thus, total surface water demand affect QDAL, we set EFR to be alternatively equal to half of $\overline{Q_{nat}}$, or zero (Section 3.2 and Section 4.2). These alternatives represent situations in which humans wish to protect freshwater biota less, or not at all, so the total surface water demands and, thus, consequently streamflow deficits are lower.

2.3.2 Anomaly

The quantification of the streamflow anomaly (p_Q) is computed with based on the interannual variability of monthly aggregated streamflow (Q_{ant}) values for each calendar month. The unusualness of a streamflow drought is better captured by a standard cumulative distribution function that can reproduce the statistical structure of streamflow (Q_{ant}) compared to a standard distribution function reproducing the statistical structure of streamflow deficit (d_Q) due to the temporal variability of the water demand. Furthermore, the methodological consistency between the calculation of p_Q and p_{soil} is maintained, as the anomaly of soil moisture deficit (d_{soil}) is equal to the anomaly of soil moisture (SS) [mm].

In some regional streamflow drought studies (Langat et al., 2019; Sharma and Panu, 2015; Lorenzo-Lacruz et al., 2010; López-Moreno et al., 2009), the standard cumulative distribution function Pearson type III was used to fit monthly streamflow values. However, Svensson et al. (2017) rightly pointed out that the Pearson type III distribution function with a lower bound at zero is reduced to the gamma distribution function. The probability density function f and cumulative density function F of the gamma distribution function can be expressed as

$$F(Q_{ant}; a, b) = \frac{g(Q_{ant}; a, b)}{G(a)} \quad (6)$$

$$f(Q_{ant}; a, b) = \frac{b^a}{\Gamma(a)} Q_{ant}^{(a-1)} e^{-bQ_{ant}} \quad (7)$$

Formatted: Font: 10 pt

Formatted: Font: 10 pt

Field Code Changed

Formatted: Font: 10 pt

Formatted: Indent: First line: 0 cm

Field Code Changed

Field Code Changed

Field Code Changed

Formatted: Font: 10 pt

Field Code Changed

Formatted: Font: 10 pt

Formatted: Font: 10 pt

$$F(Q_{ant}; a, b) = \frac{\Gamma(Q_{ant}; a, b)}{\Gamma(a)} \quad (8)$$

where $a, b \geq 0$ are the shape parameters, $\Gamma(a)$ is the gamma function and $\Gamma(Q_{ant}; a, b)$ is the incomplete gamma function; in this form the gamma distribution supports $d > 0$. Taking into account that streamflow drought occurs when a certain streamflow value is not exceeded, while in the case of p_{soil} a soil moisture drought occurs when a certain soil moisture deficit is exceeded, the drought probability index for streamflow drought p_Q is computed as

$$p_Q = \frac{(1 - F(Q_{ant})) - 0.8}{1 - 0.8} \quad (7)$$

$$p_Q = \frac{(1 - F(Q_{ant})) - 0.8}{1 - 0.8} \quad (9)$$

280 2.4 Combining deficit and anomaly to compute SMDAI and QDAI

Water deficits (d_{soil} and d_Q) and anomalies (p_{soil} and p_Q) are combined into single deficit anomaly indicators (SMDAI and QDAI) based on the desired indicator characteristics as elaborated by Cammalleri et al. (2016). The combined drought indicator should be zero if there is either no deficit- or no anomaly-based drought. It should be equal to p and d if p and d are the same, while it should have lower values if either d or p is close to zero. Thus, following Camalleri et al. (2016)

$$SMDAI = \sqrt{p_{soil} \cdot d_{soil}} \quad (8)$$

$$SMDAI = \sqrt{p_{soil} \cdot d_{soil}} \quad (10)$$

290 and accordingly

$$QDAI = \sqrt{p_Q \cdot d_Q} \quad (9)$$

$$QDAI = \sqrt{p_Q \cdot d_Q} \quad (11)$$

295 Both SMDAI and QDAI values range from 0 to 1, where 0 corresponds to no drought hazard and 1 corresponds to extreme drought hazard. The indicator values are put into classes and coinciding drought classifications according to Table 2.

Table 2. SMDAI and QDAI ranges corresponding to drought classes.

SMDAI range /QDAI range	Drought conditions
$0 < \text{SMDAI} < 0.25$	Mild
$0.25 \geq \text{SMDAI} < 0.5$	Moderate
$0.5 \geq \text{SMDAI} < 0.75$	Severe
$\text{SMDAI} \geq 0.75$	Extreme

2.5 Fitting standard cumulative functions

Out of the total 67420 WaterGAP land grid cells, only 57043 grid cells were considered in this study. Grid cells with barren or sparsely vegetated land cover, based on the MODIS-derived static land cover input map used in WGHM (Müller Schmieid et al., 2014), together with grid cells in Greenland, were not considered. For each of these grid cells and each calendar month, we determined the best fitting beta and gamma cumulative distribution functions for monthly d_{soil} and Q_{ant} , respectively, by utilizing a combination of functions from the R packages gamlss, gamlss.dist, extremeStat and fitdistrplus.

However, as tested by the one-sample Kolmogorov–Smirnov test (KS-test) at the 0.05 significance level, for 27.12% of the grid cells in the case of d_{soil} and 39.94% in the case of Q_{ant} , the fits were rejected for all 12 calendar months. An example of an accepted grid cell and a rejected grid cell of the beta distribution function are shown in Figure S3. ~~An example of an accepted grid cell and a rejected grid cell of the beta distribution function are shown in Figure S3.~~ In the rejected grid cells, the probability of non-exceedance F_F is determined directly from the time series of 30 monthly values using the R function empirical cumulative distribution function (ECDF). The ECDF is a step function that increases by 1/30 at each of the 30 d_{soil} values of SMDAI or Q_{ant} values of QDAI (Figure S3 left). The computed F_F value of a specific d_{soil} or Q_{ant} value is the fraction of all 30 d_{soil} or Q_{ant} values that are less than, or equal to, the specific d_{soil} or Q_{ant} value. Figure S4 shows the grid cells where ECDFs had to be used to compute F_F .

3 Results

3.1 SMDAI

To clarify the interplay-relation of d_{soil} , ~~the anomaly of d_{soil} as compared to the mean monthly $d_{\text{soil,mean}}$ (which is indicated by p_{soil}~~ and SMDAI), the respective time series of these variables are shown in Figure 1 for two grid cells with rather different characteristics: a grid cell in Germany (42.25N, -121.75 E, left panels in Figure 1) and one in northeast India (88.25 E, 27.25 N, right panels in Figure 1). The values of d_{soil} in the German grid cell shows, on average over the whole

Field Code Changed

320 reference period, ~~a~~ high deficits in the summer months and low deficits only in 1-2 winter months (dashed grey line). According to the definition of p_{soil} , an anomaly-based drought hazard, as indicated by $p_{soil} > 0$ (blue line), occurs only if the actual soil moisture deficit (green line) is much higher than the mean ~~calendar month~~ seasonal values, d_{soil_mean} ; ~~this is so high per definition, that this deficit is exceeded~~ is the case in only 1 out of 5 years (Eq. 34 and Table 1). According to Eq. 810, SMDAI is always between p_{soil} and d_{soil} . In the German cell, an anomaly-based drought occurred during the unusually dry, but still
325 low deficit, winter months of 2006, resulting in an SMDAI value that was much smaller than p_{soil} . During the Central European (CEU) summer drought of 2003, SMDAI was approximately equal to p_{soil} . Thus, SMDAI appropriately indicates that anomalously low soil moisture during generally wet winter months is less of a hazard to vegetation than the same anomaly would be during generally dry summer months. The grid cell in northeast India is characterized by a low seasonality of soil moisture and a generally very high soil moisture saturation. Even for some unusually dry months (with high p_{soil}),
330 d_{soil} remains almost always below 0.25. Due to the low deficit, even in cases of high p_{soil} , SMDAI is much smaller than p_{soil} during all drought events indicated by p_{soil} . When comparing temporally averaged drought hazards between the two grid cells, SMDAI would indicate a relatively higher drought hazard for the German grid cell than for the Indian grid cell, which would not be the case if a purely anomaly-based indicator, such as p_{soil} , were used as the drought hazard indicator.

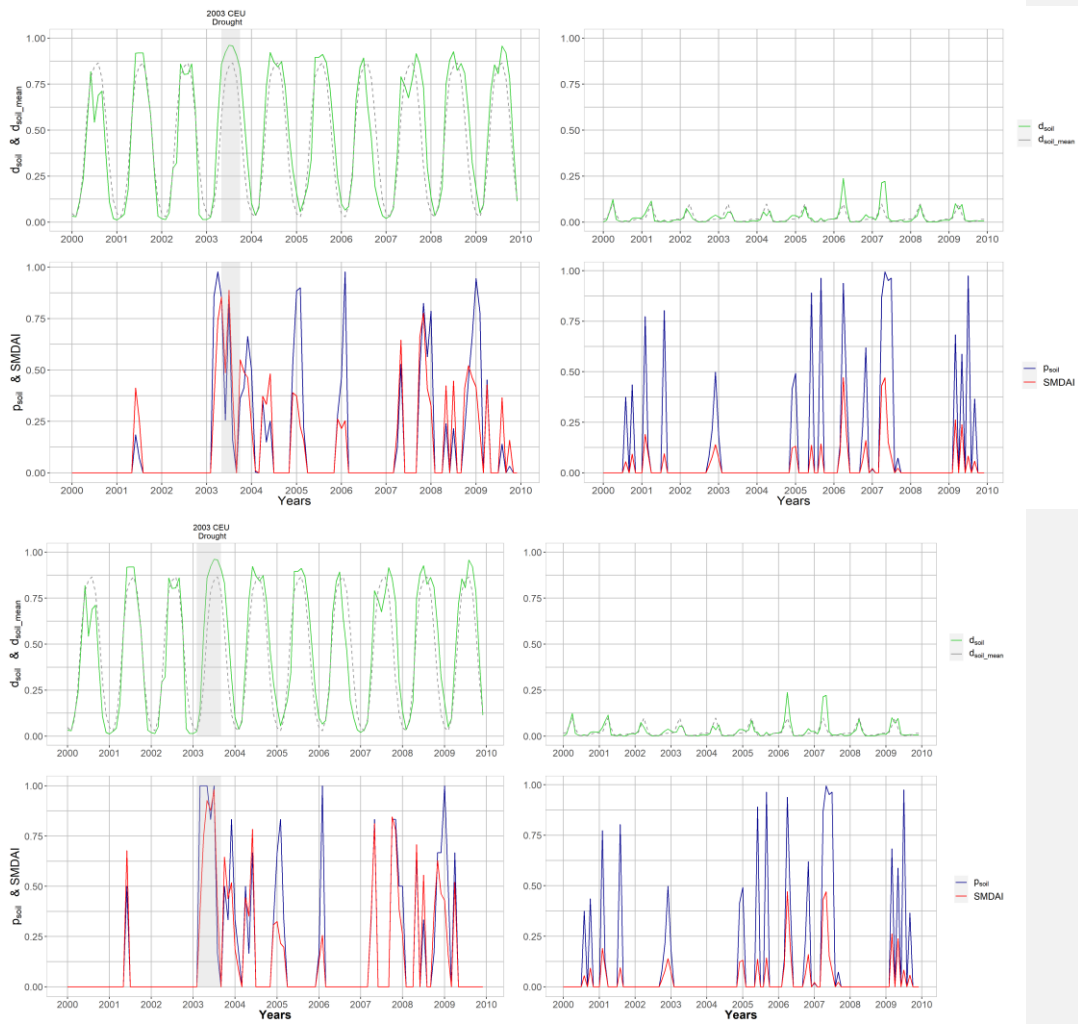
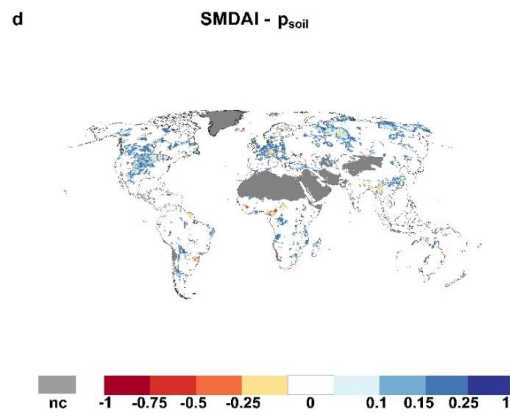
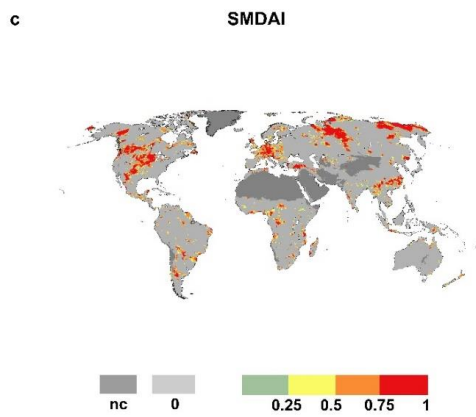
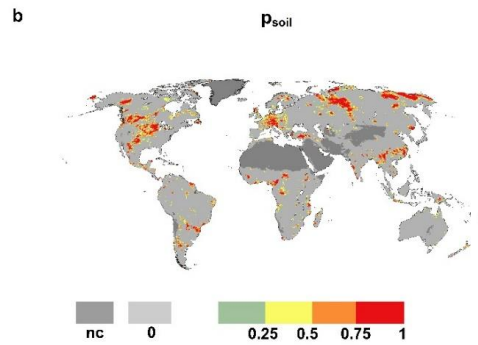
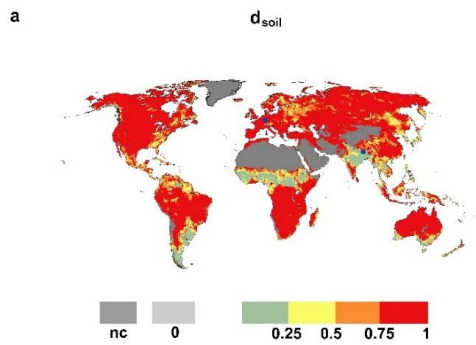
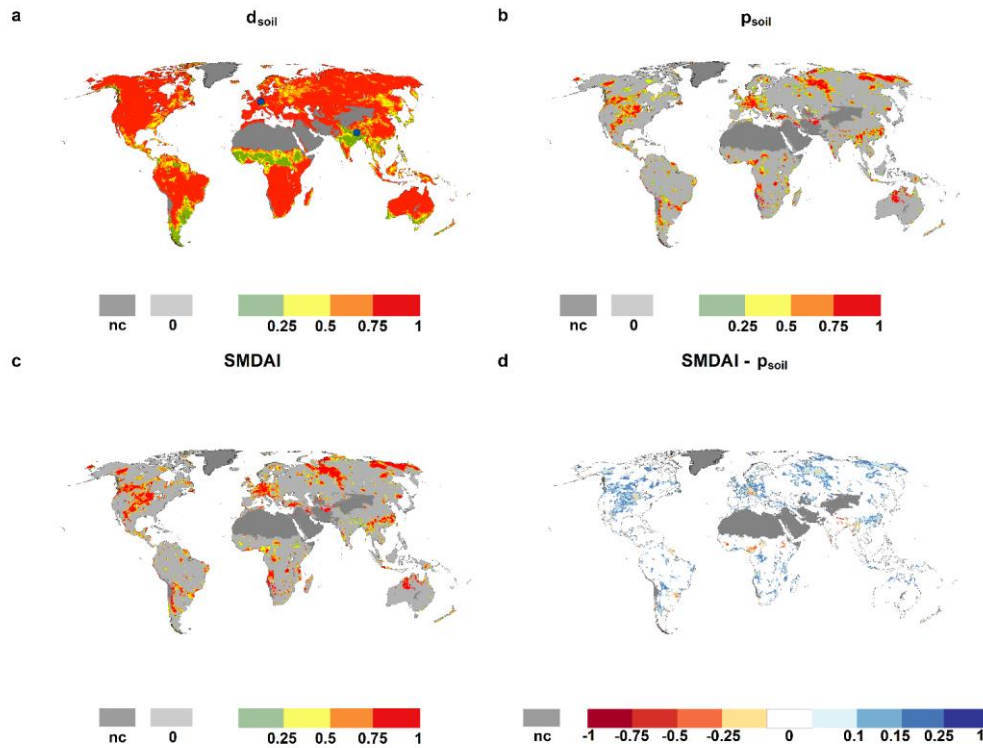


Figure 1. Soil moisture drought hazard: example of a time series (2000 – 2010) of monthly d_{soil} and mean seasonality of soil moisture deficit, p_{soil} and SMDAI (bottom) for a cell in Germany (left) and northeast India (right). The central European (CEU) drought in 2003 is indicated.

340 The relationship between SMDAI, p_{soil} , and d_{soil} can be explored further by using global indicator maps for a specific month, e.g., August 2003 (Figure 2). WaterGAP computes soil moisture deficits of 75% or more in most grid cells, while low deficits occur only in a few areas, where August belongs to the rainy season, e.g., the Sahel region and the monsoon areas in India. ~~do low deficits occur~~ (Figure 2a). In each grid cell, p_{soil} is, per definition, zero in 80% of all August months. Therefore, in any month, approximately 80% of the grid cells indicate no drought and ~~p_{soil}~~ equals 0 (Figure 2b). Only
345 grid cells with a non-zero p_{soil} have a non-zero SMDAI (Figure 2c). ~~F~~ for example, southeast India shows extremely high d_{soil} values, but as there is no anomalously high soil moisture deficit except for ~~in~~ a few grid cells where p_{soil} is mostly zero, SMDAI is also mostly zero. ~~T~~ and, thus, no soil moisture drought hazard is ~~detected~~ indicated. The difference between SMDAI and p_{soil} is shown in Figure 2d. ~~I~~ in most grid cells with differences, SMDAI is higher than p_{soil} due to high d_{soil} . Focusing on central Europe, SMDAI (in Figure 2c) correctly ~~detects~~ indicates the summer drought of 2003, documented in the EM-
350 DAT International Disaster Database (<http://www.emdat.be>), the European Drought Reference database (<http://www.geo.uio.no/edc/droughtdb>) and in Spinoni et al. (2019). The location of grid cells from Figure 1 ~~are~~ is represented in Figure 2a with blue points drawn at the ~~center~~ centre of each grid cell. During northern hemisphere winter months, soil moisture deficits are lower, for example, in Europe and the eastern part of North America, but high in most snow-dominated northern high-latitude regions, with corresponding effects for the relationship between p_{soil} and SMDAI (see Figure S54
355 showing the drought situation in December 1999). ~~I~~ in Europe and the eastern part of North America, for example, SMDAI is smaller than ~~p_{soil}~~ p_{soil} (Figure S54d).

Field Code Changed



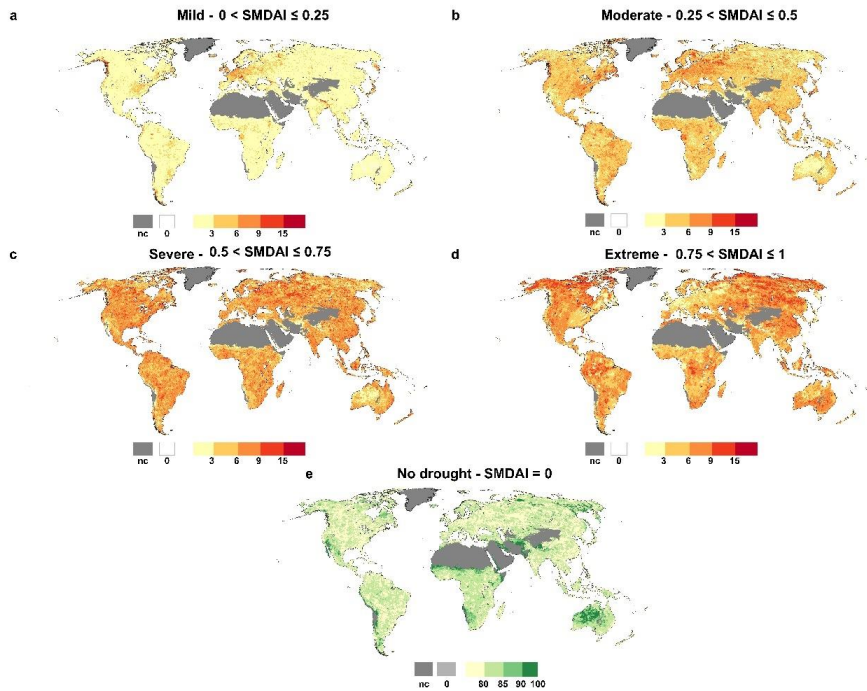


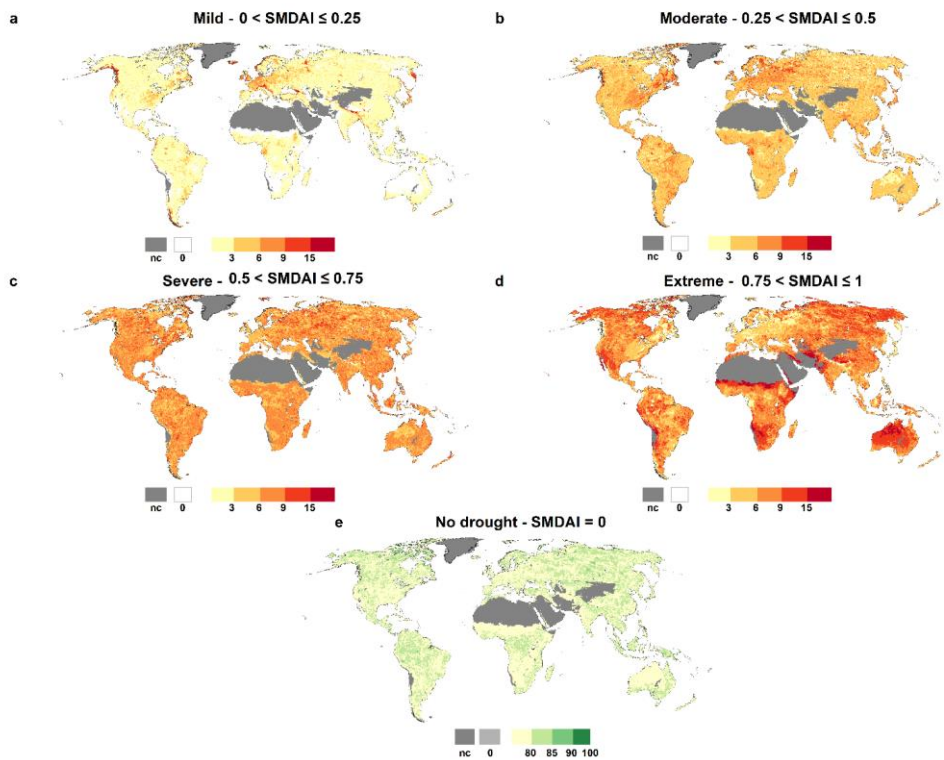
360 Figure 2. Global maps of d_{soil} , p_{soil} , SMDAI and the difference between SMDAI and p_{soil} for August 2003. Blue points in (a) represent the location of German and Indian grid cells from Figure 1 and nc are grid cells that are not computed due to land cover.

365 Figure 3 shows the frequency of occurrence of the four SMDAI drought classes specified in Table 2 and of the no-drought condition (SMDAI = 0) during the reference period 1981-2010. SMDAI is zero in about 80% of the cases, following p_{soil} as monthly soil moisture almost never reaches the maximum soil moisture capacity, in more than 80% or more of all months as p_{soil} should be zero in 80% of the months of the months as p_{soil} should be zero in 80% of the months (Figureure-3e). Values larger than 80% occur where and if d_{soil} were is zero while p_{soil} often zero, SMDAI would be zero more often than p_{soil} is not, which occurs in particular in very dry areas. However, Figure 3 shows larger values in the dry regions and, thus, we believe that the higher frequency of no-drought conditions and constant low-occurrences of drought-hazards in areas

370 ~~with high mean soil moisture deficits, such as the Sahel region, are may be due to the imperfect fits of the applied CDFs.~~
Extreme soil moisture drought hazards (Figure 3d) occur with a relatively high frequency in the ~~Mediterranean northwestern~~
~~parts of Australia and southeastern parts of Africa, parts of central Australia and South Africa.~~ Regions with mostly low soil
moisture deficits, such as central and eastern European countries and ~~the~~ eastern USA, show very low occurrence frequencies
of extreme drought hazards and more often than other regions a moderate drought hazard (Figure 3b). Snow-dominated regions,
375 such as parts of Russia and Canada, show a relatively high frequency of extreme soil moisture droughts due to the high values
of simulated soil moisture deficits created by the lack of liquid water to infiltrate the soil during the winter months and the
temperature-driven seasonal shifts of snow melts and, thus, infiltration of water into the soil.

Formatted: Not Highlight





380

Figure 3. Frequency of occurrence [%] of different soil moisture drought classes during the period 1981-2010, as defined by SMDAI (Table 2) and nc are grid cells which not computed due to land cover.

3.2 QDAI

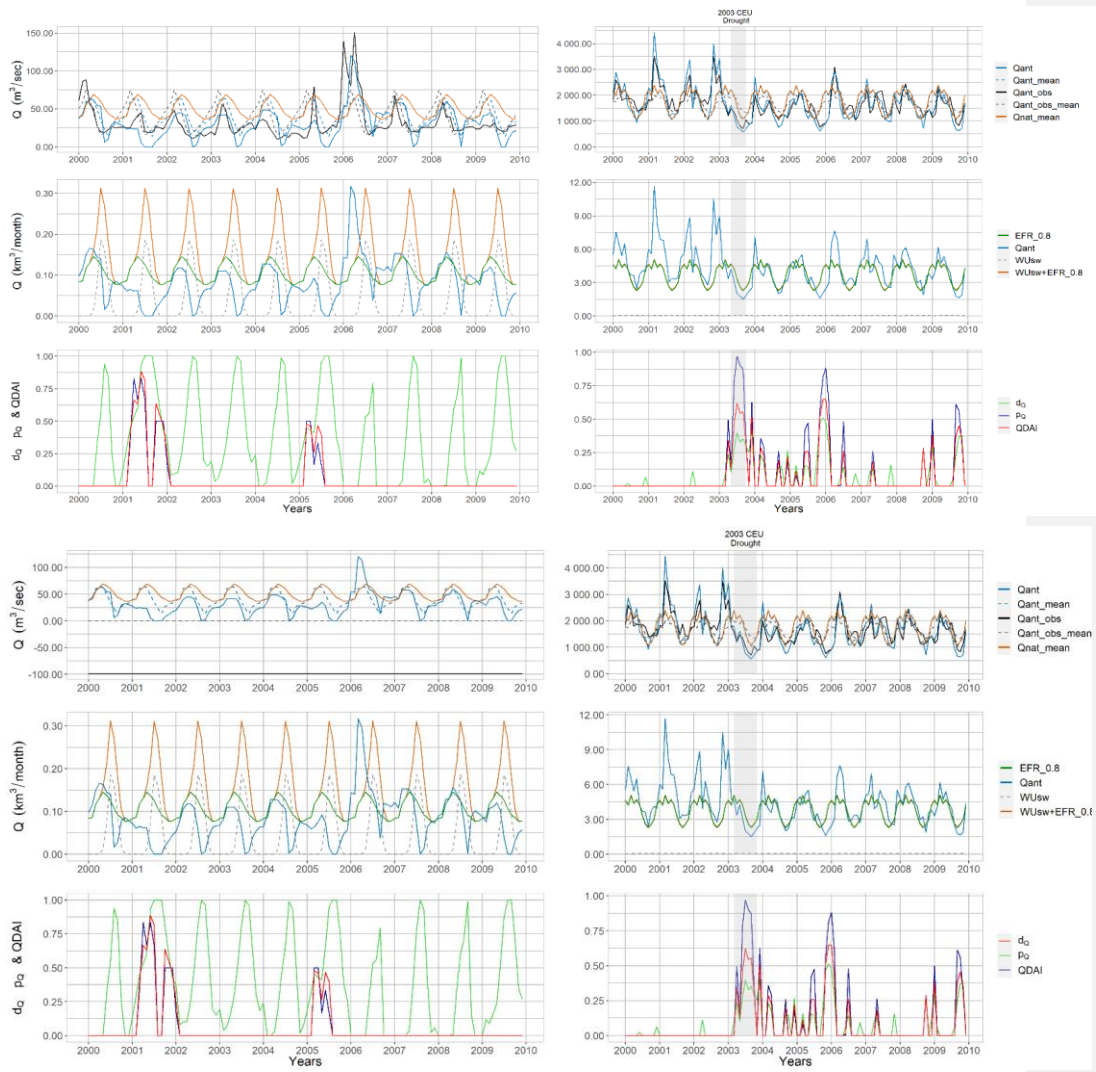
385 The QDAI indicates the drought hazard to for the surface water supply required for satisfying human water demand (WU_{sw}), assuming the water suppliers also take into consideration the water demand by freshwater biota (~~EFREFR~~). The deficit component of QDAI (d_Q) is the relative difference between the total surface water demand and streamflow, while the anomaly component (p_Q) is based on the unusualness of streamflow. QDAI depends on more individual variables than SMDAI. Figure 4 shows their interplay-relation for two grid cells with different characteristics of human surface water demand as compared to streamflow. In the grid cell in the western USA, where streamflow of the Klamath River is observed in Keno

390 (42.25N, -121.75 E, left panels of Figure 4), water demand (~~is~~ mostly for irrigation, ~~with a mean of (i.e., 0.038 km³ month⁻¹ temporal mean)~~ is high compared to the relatively small streamflow (~~i.e., 0.105 km³ month⁻¹ temporal mean~~). In the grid cell in Germany, human surface water demand ~~of (i.e., 0.056 km³ month⁻¹ temporal mean)~~ is small as compared to the rather high streamflow ~~of the Rhine of (i.e., 4.6 km³ month⁻¹ temporal mean), of the Rhine where the streamflow is measured in at~~ Mainz (49.75 N, 8.25 E, right panels of Figure 4).

395 In the USA grid cell, the difference between the mean monthly streamflow under the naturalized condition (Q_{nat_mean}) and mean monthly simulated streamflow (Q_{ant_mean}) is high, especially in the growing period, due to ~~the high large anthropogenic anthropogenic extraction abstractions~~ of streamflow water ~~in the drainage basin of the grid cell~~ (observed in the topmost plot). While the observed (Q_{ant_obs}) and simulated (Q_{ant}) streamflow show a reasonable correlation, ~~WaterGAP appears to overestimate streamflow depletion by human water use in the summers. Characterized by a high seasonality of anthropogenic surface water demand, WU_{sw} (dashed grey line in centercenter plot) and generally unfulfilled surface water demand (i.e., $WU_{sw} + EFR_{0.8}$, orange line in centercenter plot) result in frequent high summer d_Q (green line of the bottom plot). In addition, an-the anomaly-based drought hazard indicated by $p_Q > 0$ (dark blue line) indicates high summer-values occurring as if Q_{ant} is, which are much lower than the mean seasonal value (Q_{ant_mean}), which happens to occur, during the 10 years considered in Figure 4, in months with appreciable deficits. Hence, QDAI, which is always between p_Q and d_Q (Eq. 129), is rather similar to p_Q in this example detects extreme streamflow droughts incurred by high water extractions for irrigation during the summer months.~~

400 If water suppliers ~~assumed that the river ecosystems do not require 80% of naturalized streamflow for their well-being but only 20%, do not take into account when extracting water, the water that needs to remain in the river for the river ecosystem (EFR_EFR is assumed to be zero), the streamflow deficit (i.e., $WU_{sw} + EFR_{0.2}$, orange line in the centercenter plot of Figure S5) decreases (Figure S65). Hence, QDAI values decrease for all summer droughts as can be clearly observed in the summer droughts of 2000 and 2008, and-However, the winter droughts in 2001 and 2005, which that were detected when considering the larger EFREFR, are no longer identified.~~

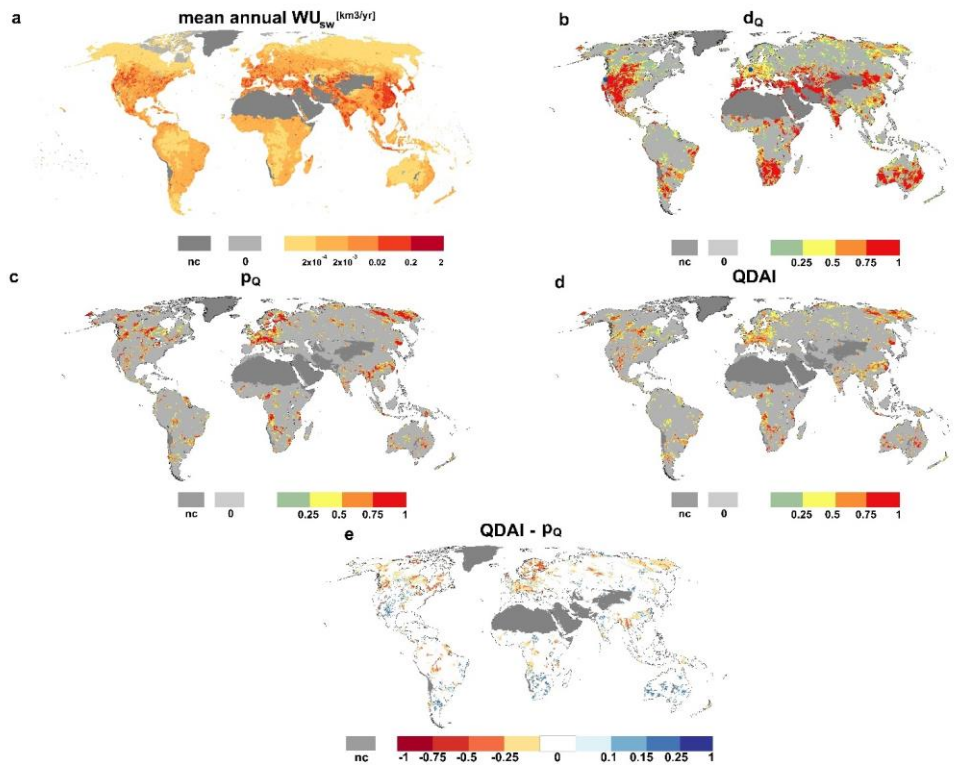
410 In the German grid cell (~~the~~ right panels in Figure 4), the relatively low anthropogenic surface water demand results in almost identical values of Q_{nat_mean} and Q_{ant_mean} (lines overlap in the top plot), ~~as well as the and~~ total surface water demand ~~and-is very similar to~~ EFR (lines overlap in the centercenter plot). Non-zero d_Q values (bottom plot) are mainly computed if Q_{ant} is lower than EFREFR, such as during the central European drought of 2003. It is sensible to consider this type of situation as a drought hazard as water supply companies would have to stop any surface water abstraction if they wished to protect the river ecosystem. If the water supply companies do not stop any surface water abstraction (EFR_0.2), then they would not suffer from any hazard, even during a drought similar to the 2003 central European drought (right panels Figure S65). Differing from a purely anomaly-based drought hazard indicator, the QDAI indicates much stronger droughts in the USA grid cell when compared to the German cell, as it indicates a drought hazard only if surface water demand, the sum of human and the ecosystem water demand, is higher than the streamflow.



425 Figure 4. Streamflow drought hazard: example of a time series (2000 – 2010) of monthly surface water demand, surface water supply, and mean seasonality of surface water supply, as well as d_0 , p_0 and QDAI (bottom) for a cell in the USA (left) and Germany (right).

The global streamflow drought ~~related hazard~~ maps for August 2003 (Figure 5) help to illustrate the global variations of QDAI as a function of its components p_Q and d_Q , which again depends on the human surface water demand WU_{sw} .

430 Streamflow deficits are not restricted to areas with high mean annual WU_{sw} during the period 1981-2010 (Figure 5a), but can be greater than 75% in regions such as South Africa where Q_{ant} is low (Figure 5b). ~~Unlike factors of~~ Different from soil moisture drought, p_Q and d_Q are strongly correlated (Figure 5c). This is due to the fact that total surface water demand is dominated in many grid cells by ~~EFREFR~~, which is a fraction of Q_{nat} . In the ~~EFREFR~~-dominated cells, the mean monthly Q_{ant} is very similar to the mean monthly Q_{nat} , such that d_Q is then approximately the difference between mean monthly Q_{ant} and Q_{ant} :
435 ~~this difference is also the basis for computing~~; ~~this is represented~~ by p_Q . QDAI (Figure 5d). ~~QDAI is and is found to be~~ mostly ~~smaller than~~ y -less than p_Q (Figure 5e). The 2003 central European drought hazard for the surface water supply for humans (Figure 5d) is, at least in many parts of Germany, less pronounced than the soil moisture drought hazard for vegetation (Figure 2c). Figures 5c-e also indicate the grid cells with $Q_{ant} = 0$. ~~If streamflow in a grid cell is zero in 20% or more of all August months (left panel of Figure S7), p_Q and thus QDAI is zero because the zero streamflow is not an anomaly that occurs~~
440 ~~in less than 1 out of 5 years.~~



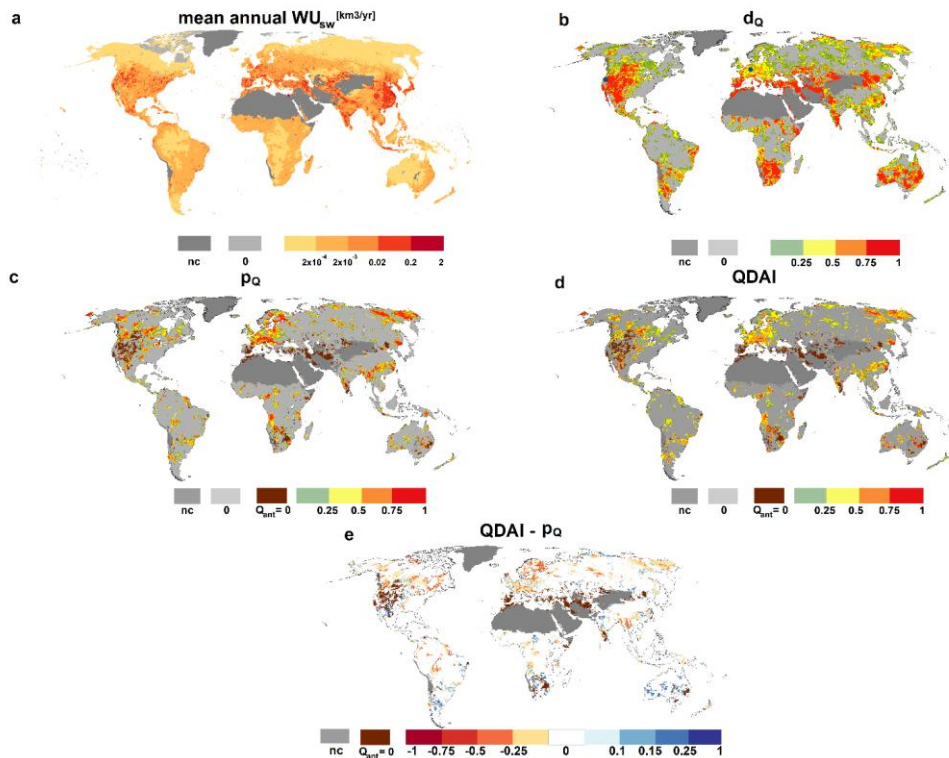


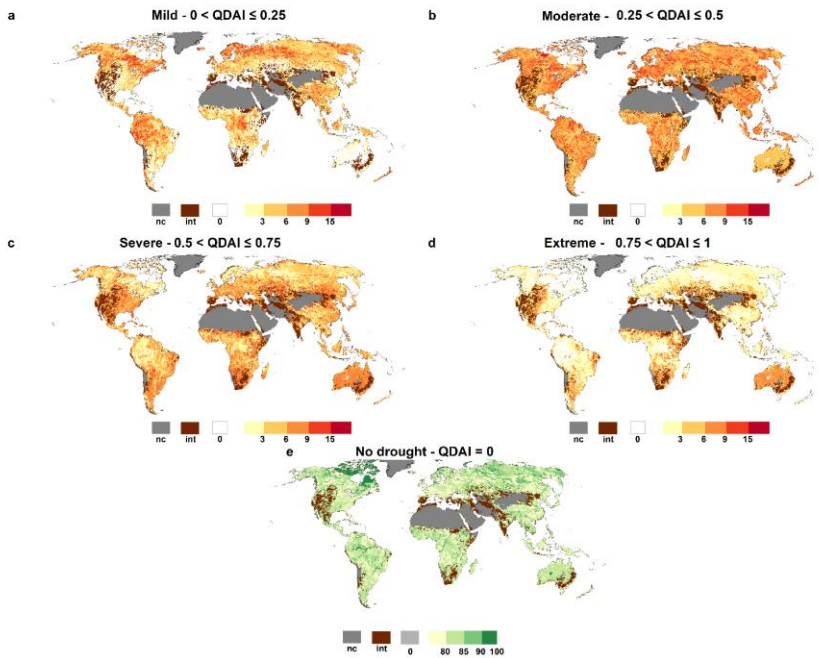
Figure 5. Global maps of mean annual WU_{sw} , d_Q , p_Q , QDAI and the difference between QDAI and p_Q for August 2003. Blue points in (b) represent the location of the German and USA grid cells from Figure 4. Grid cells with $Q_{ant} = 0$ are indicated; nc: QDAI is not computed due to land cover.

In contrast to SMDAI, the frequency of occurrence of no-drought conditions according QDAI is larger than 80% in grid cells particularly with large rivers and barely any human water use, such as the Amazon River in South America, the Congo River in Africa, and the Ob River in Russia (Figure. 6e), where the deficit is often zero. Besides, grid cells with intermittent flows also show a high percentage of no-drought conditions, if for any calendar month there are at least six months (i.e., at least 20% of the months) with $Q_{ant} = 0$ (Figure S7). In these grid cells, no-drought conditions are due to zero streamflow is not an anomaly that occurs in less than 1 out of 5 years. This type of intermittent grid cells, where $Q_{ant} = 0$ for least 20% of the months of any calendar month are marked separately in Figures 6c-e. Extreme streamflow drought hazard for human water supply (Figure 6d) occurs most often in regions with high streamflow deficits (compare Figure 5b), such as South Africa and

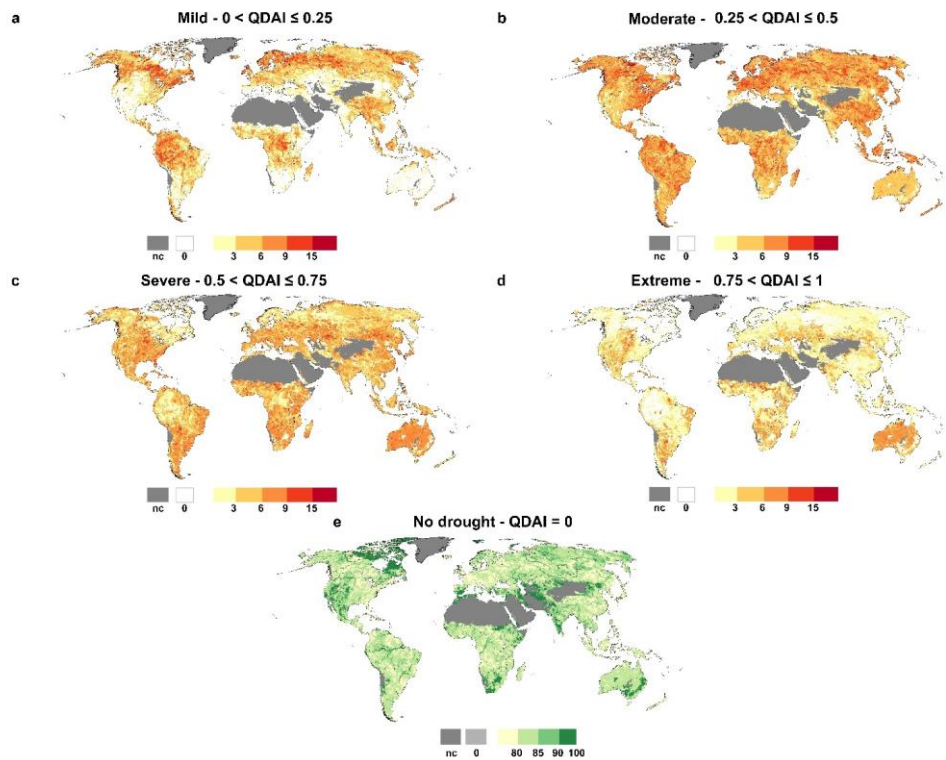
455 parts of southeastern Australia, i.e., regions with low streamflow and relatively high surface water abstractions, mainly for
 irrigation (Figure 5a). Regions with low water human surface water abstractions such as northern Canada and the Amazon and
 Congo basins, show an exceptionally high occurrence of mild drought hazards (Figure 6a).

460 **Figure 5. Global maps of mean annual WU_{sw} , d_Q , p_Q , QDAI and the difference between QDAI and p_Q for August 2003. Blue points in (b) represent the location of the German and USA grid-cells from Figure 4.**

465 Differing from SMDAI (Figure 3), the no drought conditions, as identified using QDAI, occur more often than 80% of the time as d_Q is often zero, in particular, in very large rivers with scarcely any human water use such as the Amazon river in South America, the Congo river in Africa and the Ob river in Russia; these are clearly visible in Figure 6e. Extreme streamflow drought hazard for human water supply (Figure 6d) occurs most often in regions with high streamflow deficits (compare Figure 6b), such as South Africa and southeastern Australia, i.e., regions with low Q streamflow and relatively high surface water abstractions for irrigation. Regions with low to moderate water human surface water demand (Figure 5a), such as northern Canada and the Amazon and Congo basins, show an exceptionally high occurrence of mild drought hazards (Figure



6a).



470

Figure 6. Frequency of occurrence [%] of different streamflow drought classes during the period 1981-2010 as defined by QDAI (Table 2). Grid cells where for any calendar month there are at least six months with $Q_{ant} = 0$ are indicated as int and grid cells which are not computed due to land cover are indicated as nc. Figure 6. Frequency of occurrence [%] of different streamflow drought classes during the period 1981-2010 as defined by QDAI (Table 2).

475 4 Discussion

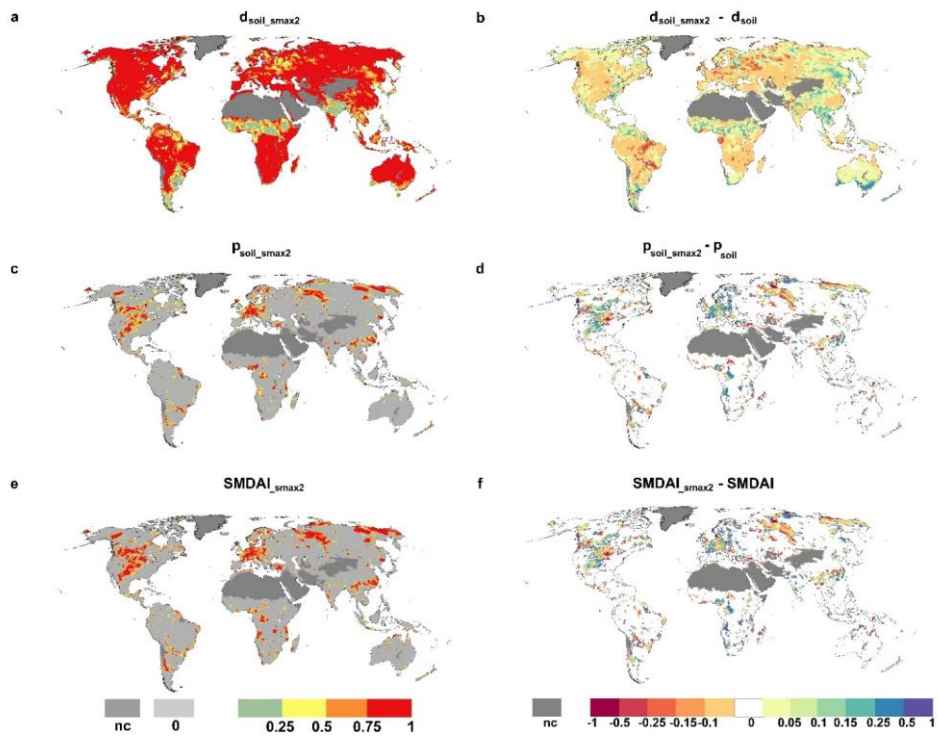
4.1. Analysis of SMDAI and QDAI components

4.1.1 Sensitivity of SMDAI to the S_{max} values assumed in WaterGAP

S_{max} is one of the key components for computing SMDAI. WaterGAP calibration and validation studies have indicated that S_{max} may be underestimated in WaterGAP by a factor of two or more (Hosseini-Moghari et al., 2020). In

Field Code Changed

480 order to understand the sensitivity of SMDAI to changes in S_{\max} , we ran a version of WaterGAP in which S_{\max} was doubled
($S_{\max 2}$). Figure 7 presents global maps of $d_{\text{soil}_S_{\max 2}}$ (Figure 7a), $p_{\text{soil}_S_{\max 2}}$ (Figure 7c), and $\text{SMDAI}_{S_{\max 2}}$ (Figure 7e) for
~~the August~~ 2003, and the change in each parameter with respect to the standard WaterGAP output i.e., the difference between
parameter computed using $S_{\max 2}$ and S_{\max} (Figure 7b, 7d, and 7f). With $S_{\max 2}$, more amount of soil moisture
is kept in the soil and soil deficits, expressed relative to S_{\max} , can be observed to increase or decrease with doubled
485 S_{\max} (Figure 7b). Differences are mostly small except for scattered grid cells in which the soil moisture deficit decreases
by more than 50 percentage points. Such cells are also found in central Europe where, under the heavy drought conditions of
August 2003, computed deficits d_Q are generally smaller in the case of doubled S_{\max} ; in this region, p_{soil} increases
in the case of doubled S_{\max} (Figure 7d). Globally, p_{soil} increases or decreases in some grid cells by more than 50
percentage points. Equally, for SMDAI, the sensitivity to doubled S_{\max} is low for most grid cells but can be greater for a
490 few (Figure 7e).



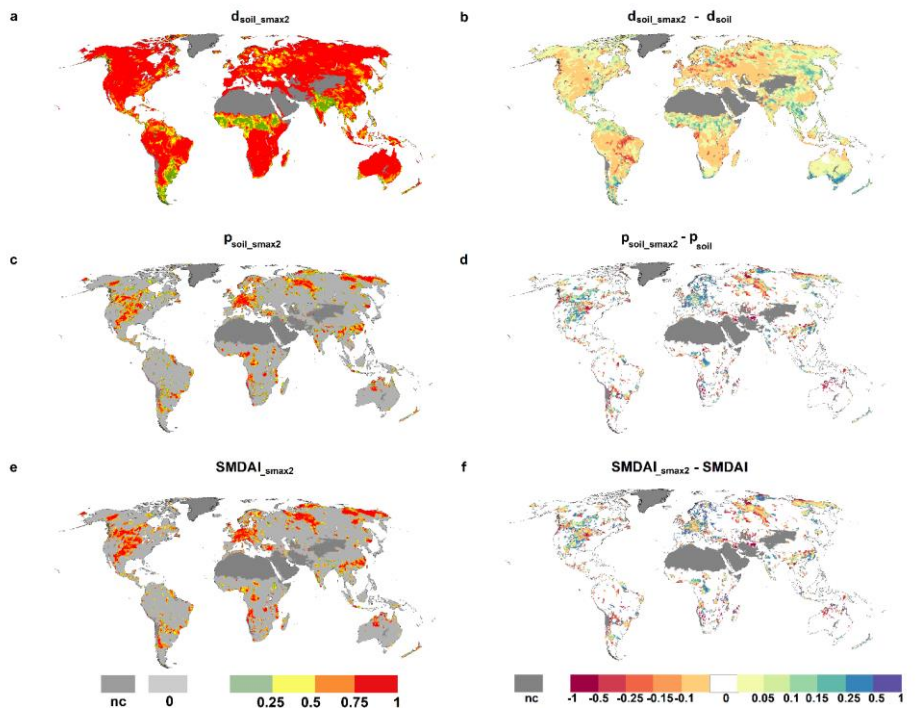
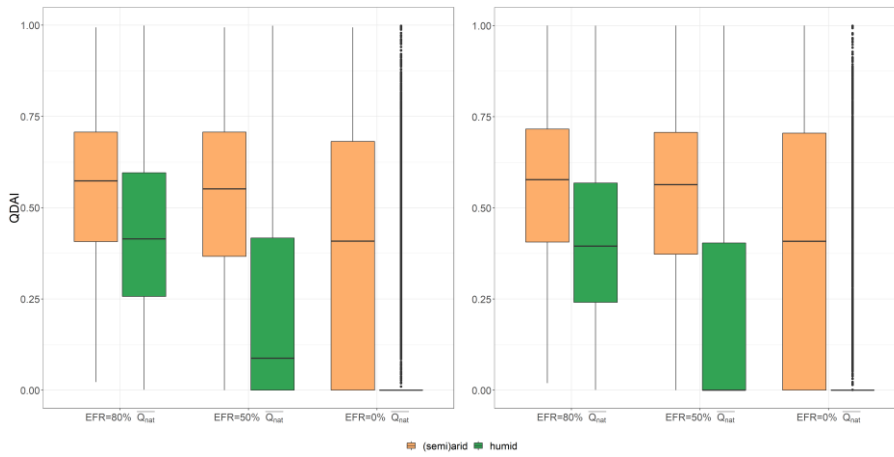


Figure 7. Spatial representation of d_{soil} , p_{soil} and SMDAI computed with S_{max2} are presented in the left panel, and, in the right panels, are the differences in these d_{soil} , p_{soil} , and SMDAI compared to the results computed with the standard version of WaterGAP for August 2003 as well as nc are grid cells which not computed due to land cover.

4.1.2 Sensitivity of QDAI to different assumptions about EFR

The streamflow drought hazard for water supply indicated by QDAI depends on how EFR_{EFR} is computed, i.e., given that the protection of river ecosystem as one of the important conditions is included. In Figure 8, we compare the global distribution of QDAI values among the 57043 0.5° grid cells that are computed for alternative EFR_{EFR} , assuming that either 80% or 50% of mean monthly natural streamflow is required to remain in the river for the well-being of the river ecosystem, or that there is no EFR_{EFR} at all that needs to be considered when the decisions about river water abstractions for water supply are made. We consider the two months of August and December 2003 and distinguish between humid and (semi)arid grid cells (Figure-S68). The boxplots show that a drought hazard in humid areas is only identified if the existence of an EFR_{EFR} is acknowledged. If water suppliers in humid areas assume that all water in the river can be abstracted, they will very rarely be

505 unable to satisfy their demand. In humid grid cells, QDAI increases strongly with the selected ~~EFREFR~~, which means that
with increasing consideration of the water requirements of the river ecosystems, drought hazards to the water supply increase,
i.e., there are more situations where water abstractions would have to be reduced to keep enough water in the river for the
ecosystems to thrive. In (semi)arid regions, QDAI is already very high, even without acknowledging any water requirement
of the river ecosystem. As in humid regions, QDAI increases with increasing ~~EFREFR~~. As can be expected, QDAI, for
510 example, as shown by the median, is overall somewhat higher in the northern hemisphere summer month of August 2003 than
in December 2003, but the impact of alternative ~~EFR_EFR~~ assumptions is similar. Figure 8 also clearly shows that water
suppliers in (semi)arid and arid regions suffer from drought hazards much more strongly than water suppliers in humid areas
due to the much higher ratio of water demand to streamflow.



515

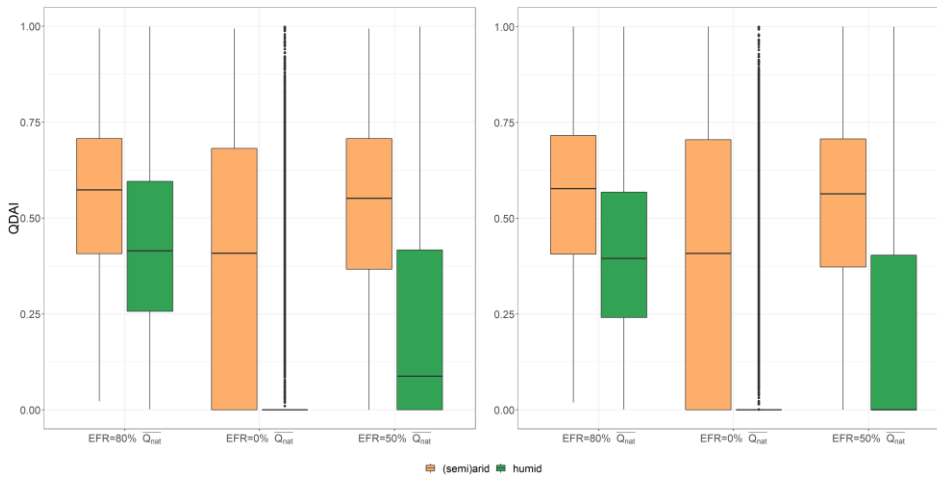


Figure 8. Global distribution of QDAI in August 2003 (left) and December 2003 (right), computed with alternative assumptions about EFR for grid cells with humid and (semi)arid conditions.

Further differences between different QDAI values computed for alternative EFR are explored for two widely known drought events, the i.e., South Asian drought of 2009 (Neena et al., 2011) and the North American drought of 2002 (Seager, 2007). Figure 9 presents the spatial extent of both the droughts detected by QDAI at a continental scale (left panels of figure 9) for August 2009 and March 2002, respectively. Further, time series plots (in the right panels of Figure 9) for an Indian

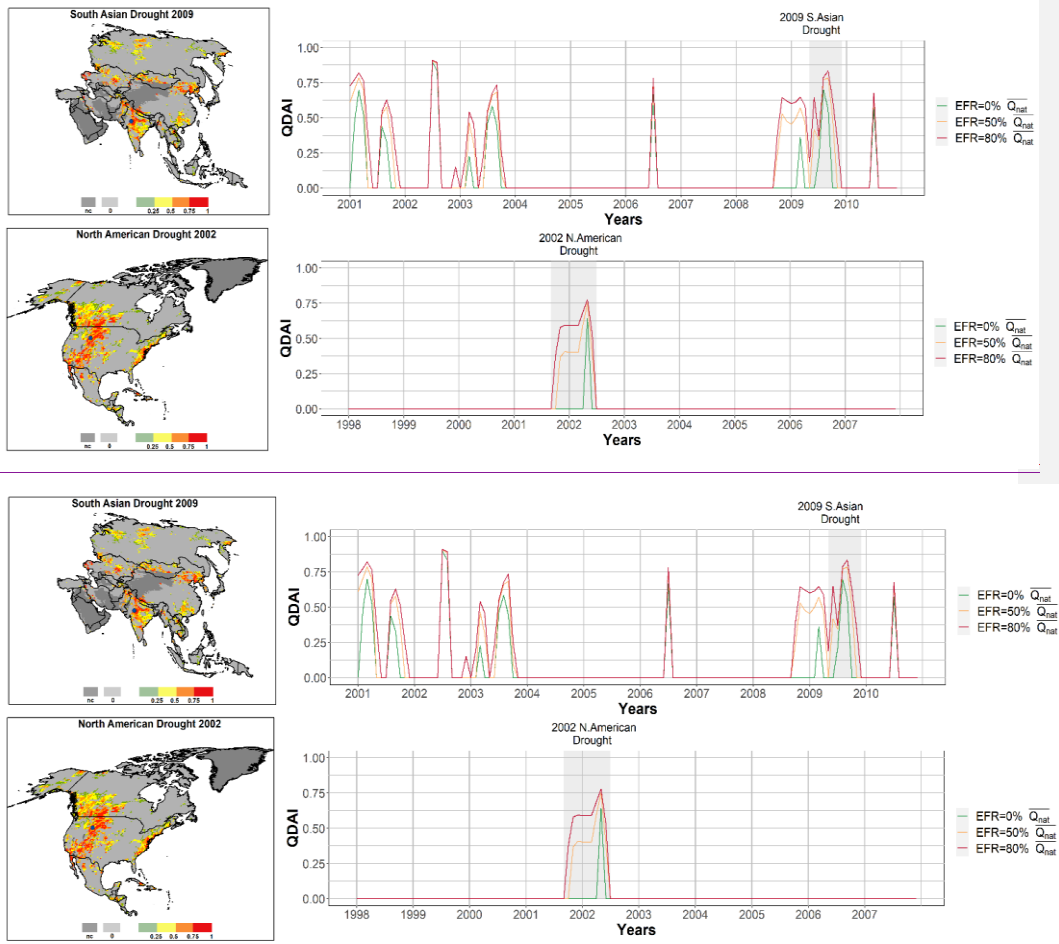
520

- Field Code Changed
- Field Code Changed
- Formatted: English (United States)
- Formatted: English (United States)
- Formatted: English (United States)

525 grid cell (75.75 E, 24.75 N top panel) as well as another for a USA grid cell (-110.75 E, 44.25 N bottom panel), as well as
another for a USA grid cell (-110.75 E, 44.25 N bottom panel), are also presented in figure 9 which provide a better
530 understanding of the sensitivity of QDAI to EFR. As expected, QDAI values calculated with no EFR at all, i.e., EFR =
0% ($\overline{Q_{\text{nat}}} = 0$ (presented in green)) a line is observed to detect lower QDAI values are lower and drought periods shorter than
if it is assumed that water needs to remain in the river for the well-being of the ecosystems as well as span of drought compared
to QDAI with EFR, assuming that either 80% or 50% of mean monthly natural streamflow is required to remain in the river
for the well-being of the river ecosystem. Interestingly, short but severe drought in the However, in Indian grid cell with
530 frequent streamflow droughts, it is observed that for smaller and more severe droughts, such as in 2002, 2006, and 2010 have
almost equal QDAI values and span for all three EFR alternatives.

Formatted: English (United States)

Formatted: English (United States)



535

Figure 9. Continental maps of QDAI for Asia and Northern America for August 2009 and March 2002 respectively (left panels) with blue points representing showing the location of the Indian and USA grid cells. Time series of different QDAI with alternative EFR (right panels) for Indian grid cell for 2001-2010 and USA grid cell for 1998 – 2007 and nc are grid cells which are not computed due to land cover.

540

4.2.3 Comparing QDAI to the Standardized Streamflow Index (SSFI) (SSFI)

The Standardized Streamflow Index (SSFI) is a well-known anomaly-based drought indicator introduced by Modarres (2007) that is computed separately for each calendar month, similar to the Standardized Precipitation Index (SPI) (Mckee et al., 1993), as

$$SSFI = \frac{Q_{anti} - \overline{Q_{ant}}}{\sigma} \quad (10)$$

$$SSFI = \frac{Q_{anti} - \overline{Q_{ant}}}{\sigma} \quad (13)$$

where Q_{anti} [$\text{km}^3 \text{ month}^{-1}$] is the streamflow value at time interval i , $\overline{Q_{ant}}$ is the long-term mean of the streamflow values and σ is the standard deviation of the streamflow values used in calculating the long-term mean. Like p_Q , SSFI assumes biota and humans are accustomed to the seasonal and interannual variability of the streamflow. In order to quantify the added value of QDAI, we compared QDAI values to SSFI values computed with a 1-month timescale. The anomaly of streamflow in SSFI was computed in the same manner as for p_Q , by fitting the gamma cumulative distribution function for monthly Q_{anti} . It was which is then transformed into Gaussian distribution by calculating the mean, standard deviation, as well as using the approximate conversion provided by Abramowitz and Stegun (1965); this is also used by Kumar et al. (2009). Figure 109 shows three grid cells characterized with by rather different values of the ratio R of long-term average annual WU_{sw} to long-term average annual Q_{ant} : high (Vietnam, 10.75N, 107.25E in Figure 910a), moderate (south-east USA 31.75N, -84.75E in Figure 109b) and low (Russia, 63.75 N, 136.75E in Figure 910c).

As would be expected, p_Q and SSFI show an equivalent behavior in all grid cells as they are based on the same streamflow data, do not use any additional information and can be mathematically transformed from one to the other (Table 1). In contrast, QDAI is based additionally on estimates of the grid cell's specific human surface water demand and assumptions on EFR. A comparison of SSFI and QDAI is, therefore, essentially a comparison of p_Q and QDAI. If R is very small, such as in the case of the Russian grid cell, with $R = 3.5 \times 10^{-6}$ (Figure 109c), p_Q and QDAI is very are very similar to p_Q , while d_Q are is very similar to EFR, being 80% of the mean monthly Q_{nat} (see explanation in Section 3.2). For the Vietnamese grid cell with a high R value of 0.143, QDAI does not interpret the anomalously low streamflow values in late-December 2003 and December 2005 as a drought hazard due to the low human water demand for surface water in December. Globally averaged, the fraction of months under drought during 1981-2010 is 16.0% according to QDAI and 19.1% according to SSFI. This reflects that QDAI only identifies a drought condition if there is, in addition to the anomalously low flow, a water deficit. Further, considering every value of $QDAI > 0$ and $SSFI < -0.84$ as an indication for an individual drought hazard, we

Formatted: Font: (Default) +Headings (Times New Roma

Field Code Changed

Field Code Changed

Field Code Changed

Formatted: Font: 10 pt

Field Code Changed

Formatted: Font: 10 pt

Formatted: Font: 10 pt

Formatted: Indent: First line: 0 cm

Formatted: Indent: First line: 0 cm

Field Code Changed

Field Code Changed

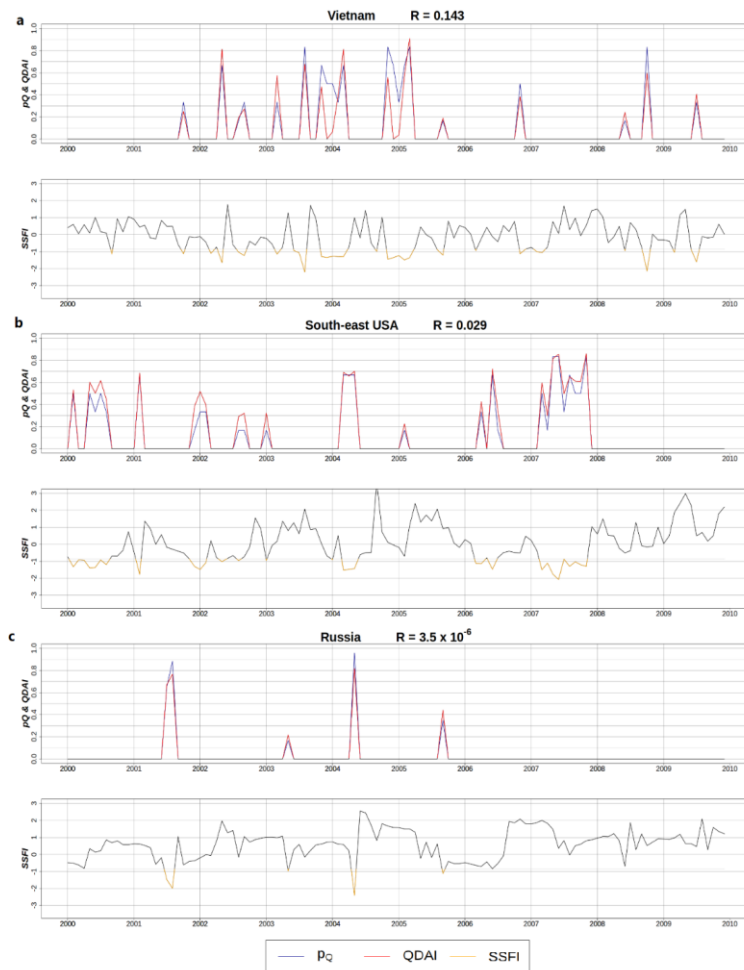
Field Code Changed

Field Code Changed

Formatted: English (United States)

570 find SSFI indicates number of drought hazards 0.0379 times higher than QDAI on average per grid cell for the period of 1981-
2010.

Formatted: English (United Kingdom)



575 Figure 109. Time series of QDAI and *SSFI* for grid cells with different ratios of surface water abstractions to streamflow
R in three regions: a) Vietnam (10.75N, 107.25E) in (a), b) south-east USA (31.75N, -84.75E) in (b) and c) Russia (63.75

N, 136.75E) in (e). $SSFI_{SSFI}$ is shown in red if it is below -0.84 standard deviations, corresponding to a 5-year return period and a p of zero (Table 1).

4.4 Indicated propagation of drought from soil moisture to streamflow as indicated by SMDAI and QDAI

As can be expected from the flow path of water on the continents, below normal precipitation occurs before below normal soil moisture. Below normal streamflow may occur even later, but only if streamflow at a certain location is not dominated by local conditions and not conditions in a distant upstream area. This so-called drought propagation can be identified by drought hazard indicators for the respective variables (As in van Loon, (2013). Knowledge about the dynamics of drought propagation supports monitoring drought development and drought mitigation as it allows to, we also identify the translation of drought indication from anomalous meteorological conditions to hydrological conditions as drought propagation. In a typical scenario, the indication of drought as below normal availability of water is typically observed to move from precipitation, soil moisture, streamflow, and groundwater caused by natural climate variability. The determination of drought propagation in the hydrological cycle helps in better understanding the true length of drought, estimate, for example, impacts of the early meteorological drought analyzing its impact on various sectors at different stages of its propagation through the water cycle. The purely physical propagation may be expected to be best observed by purely anomaly-based indicators, e.g., using standardized drought indicators for the variables: precipitation, soil moisture, and streamflow. Here, we want to explore drought propagation from soil moisture drought to streamflow drought using the deficit-anomaly indicators SMDAI and QDAI, and monitoring its development in different climate regions around the world.

For the example of a grid cell in Germany (42.25N, -121.75 E), drought propagation is identified during the Figure 11 provides an example where drought propagation from soil moisture to streamflow is clearly observed for previously identified 2003 Central European (CEU) summer drought (Figure 11). C-By comparing the set of time series for d_{soil} , p_{soil} , SMDAI with $SSFI_{SSFI}$ and d_{QDAI} and p_{QDAI} for a grid cell in Germany (42.25N, -121.75 E) at 2002-2005 temporal scale, we observe a lag of one month in the onset of streamflow drought and a two-month delay in the termination of streamflow drought as indicated indicated by $SSFI_{SSFI}$ and QDAI compared to soil moisture drought indicated by SMDAI. Soil moisture drought lasted from March to October 2003, the streamflow drought from April to December 2003. The drought periods by SMDAI and QDAI are driven by their anomaly components As expected in both SMDAI and QDAI, the duration of respective droughts is in higher correlation with anomalous soil moisture deficit and streamflow conditions, i.e., p_{soil} and $-p_{QDAI}$ respectively. However, the highest anomaly of soil moisture is already reached May, and the highest streamflow anomaly only in August. This would indicate a time lag between peak soil and streamflow drought of three months. However, considering SMDAI and QDAI, the time lag is zero, as both peak in August, as soil moisture deficit in March is low. However, it is important to observe the severity peaks of both the droughts, i.e., SMDAI and QDAI values at the start of August 2003, are sensitive to the deficit values d_{soil} and d_{QDAI} and p_{QDAI} (as well as $SSFI_{SSFI}$) peak in the same month because human water

Formatted: English (United States)

Formatted: English (United States)

Formatted: English (United States)

Formatted: English (United States)

Formatted: English (United States)

Formatted: English (United States)

Formatted: English (United States)

Formatted: English (United States)

Formatted: English (United States)

demand in this grid cell is small as compared to the water demand of the ecosystem which is assumed to be a fraction of streamflow. An Overall, an extreme soil moisture drought event from June to August 2003 as identified by (by, SMDAI was accompanied and prolonged by values between start of June and August) prolonged by a severe streamflow drought event from July to October as identified by QDAI (by QDAI values between the start of August and October) indicates exceptionally dry summer event with a primary impact on natural vegetation, crop failure and possibly high reduction in production of goods.

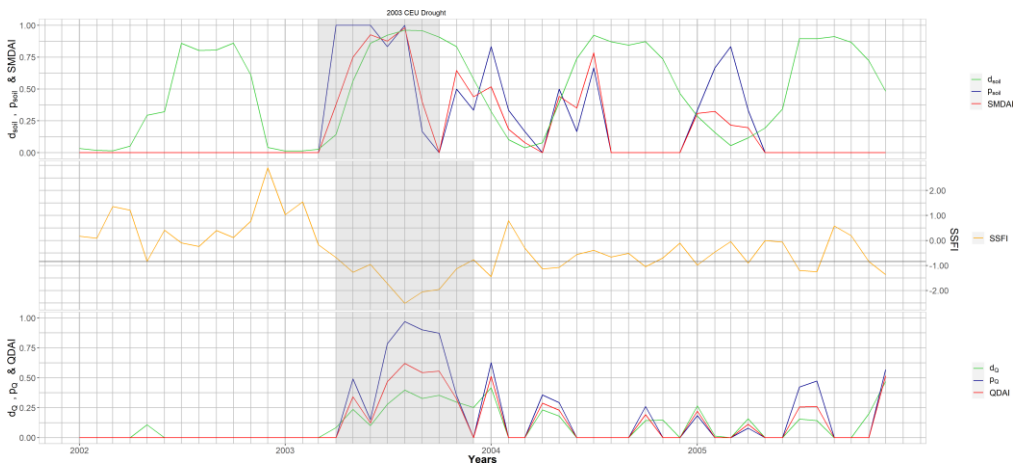


Figure 11. Drought propagation from soil moisture to streamflow: example of a time series (2002 – 2005) of monthly of d_{soil} , P_{soil} , d_Q , P_Q , SMDAI and QDAI for a grid cell in Germany.

5 Conclusion

In this paper, we presented two drought hazard indices that combine the drought deficit and anomaly characteristics: one for soil moisture drought (SMDAI) and the other for streamflow drought (QDAI). With SMDAI, which describes the drought hazard for vegetation, we achieved the simplification of the deficit-anomaly based Drought Severity Index introduced by Cammalleri et al. (2016). We transferred the DSI concept to streamflow drought, creating an indicator that specifically quantifies the hazard that drought poses for the water supply from rivers. To our knowledge, QDAI is the first-ever streamflow drought indicator that combines the anomaly and deficit aspects of streamflow drought.

The concept of SMDAI and QDAI was tested at the global scale by using simulated data from the latest version of the global water resources and using the model WaterGAP. Whereas the reliability of the computed SMDAI and QDAI values

Formatted: English (United States)

Formatted: English (United States)

Formatted: English (United States)

Formatted: English (United States)

Formatted: English (United States)

Formatted: Font: 10 pt, Font color: Auto, English (United Kingdom)

Formatted: Font: 10 pt, Font color: Auto, English (United Kingdom)

Formatted: Font: 10 pt, Font color: Auto, English (United Kingdom)

630 strongly depends on the quality of the model output, the indicators themselves have been proven to provide meaningful quantitative estimates of drought hazard that depend not only on the unusualness of the situation but also the concurrent deficit of available water as compared to demand. We found that the values of the combined deficit-anomaly drought indices are often broadly similar to purely anomaly-based indices and share with them the difficulty of dealing with intermittent streamflow regimes. ~~However,~~ they do provide more differentiated spatial and temporal patterns that and help to distinguish the degree and degree-nature of the drought hazard. QDAI can be made useful-serve as a tool for enlightening-relevantinforming water suppliers and other stakeholders about the joint drought hazard for both water supply for humans and river ecosystem, while stakeholders may adapt the EFR applied for computing QDAI in accordance ~~to~~with their valuation of ecosystem health ~~for stakeholders, who hold different perceptions on the importance of ecosystem protection, by adapting the approach for computing EFR, the amount of water that is required to remain in the river for the well-being of the river ecosystem.~~ Like all hydrological drought indicators that reflect streamflow anomaly, QDAI needs to be interpreted carefully in case of highly intermittent streamflow regimes.

640 The term “drought hazard” can be defined as the source of a potential adverse effect of an unusual lack of water on humans or ecosystems. In this sense, SMDAI and QDAI are drought hazard indicators, even if they include some elements of vulnerability to drought. Both SMDAI and QDAI are well applicable in drought risk studies. In local drought risk studies, additional indicators of ecological or societal vulnerability should be added. In regional or global drought risk studies, the inclusion of grid-scale values of QDAI and SMDAI would be beneficial as both indices contain spatially, highly ~~ly~~-resolved information on vulnerability, while most other vulnerability indicators represent spatial averages of much larger spatial units such as countries.

650 **Author contributions**

655 This paper was conceptualized by PD with input from EP. EP performed the data analysis and visualization. The original draft was written by EP and revised by PD.

Data availability

WaterGAP 2.2d model output data used in this study is available at <https://doi.pangaea.de/10.1594/PANGAEA.918447>.

Formatted: Font: Times New Roman, Font color: Auto

Formatted: Font: Times New Roman, Font color: Auto

Acknowledgments

660 We thank Dr. Hannes Müller Schmied for input and guidance on setting up the WaterGAP variant with doubled S_{\max} (Section 4.1.1) and Thedini Asali Peiris for constructive criticism of the manuscript. Also, we acknowledge funding from the German Federal Ministry of Education and Research (BMBF) for the “Globe Drought” project through its funding measure Global Resource Water (GRoW) (grant no. 02WGR1457B).

References

- 665 [Abramowitz, M. and Stegun, I. A. \(Eds.\): Handbook of mathematical formulas, graphs, and mathematical tables, Dover Publications, New York, 1965.](#)
- [Agnew, C. T.: Using the SPI to identify drought, Drought Network News \(1994 -2001\), 1, available at: <https://digitalcommons.unl.edu/droughtnetnews/1/>, 2000.](#)
- [Alcamo, J., Döll, P., Henrich, T., Kasper, F., Lehner, B., Rösch, T., and Siebert S: Development and testing of the WaterGAP 2 global model of water use and availability, Hydrological Sciences Journal, 48, 317–337, <https://doi.org/10.1623/hysj.48.3.317.45290>, 2003.](#)
- 670 [Bergez, J., Chabrier, P., Gary, C., Jeuffroy, M. H., Makowski, D., Quesnel, G., Ramat, E., Raynal, H., Rouse, N., Wallach, D., Debaeke, P., Durand, P., Duru, M., Dury, J., Faverdin, P., Gascuel-Oudou, C., and Garcia, F.: An open platform to build, evaluate and simulate integrated models of farming and agro-ecosystems, Environmental Modelling & Software, 39, 39–49, <https://doi.org/10.1016/j.envsoft.2012.03.011>, 2013.](#)
- [BoM: What is drought?, <http://www.bom.gov.au/climate/drought/>, last access: 23 June, 2020, 2018.](#)
- [Cammalleri, C., Vogt, J., and Salamon, P.: Development of an operational low-flow index for hydrological drought monitoring over Europe, Hydrological Sciences Journal, 12, 1–13, <https://doi.org/10.1080/02626667.2016.1240869>, 2017.](#)
- 680 [Cammalleri, C., Micale, F., and Vogt, J.: A novel soil moisture-based drought severity index \(DSI\) combining water deficit magnitude and frequency, Hydrol. Process., 30, 289–301, <https://doi.org/10.1002/hyp.10578>, 2016.](#)
- [Dai, A., Trenberth, K. E., and Qian, T.: A global dataset of palmer drought severity Index for 1870–2002: Relationship with soil moisture and effects of Surface Warming, J. Hydrometeor, 5, 1117–1130, <https://doi.org/10.1175/JHM-386.1>, 2004.](#)
- 685 [Döll, P., Müller Schmied, H., Schuh, C., Portmann, F., and Eicker, A.: Global-scale assessment of groundwater depletion and related groundwater abstractions: Combining hydrological modeling with information from well observations and GRACE satellites, Water Resour. Res., 50, 5698–5720, <https://doi.org/10.1002/2014WR015595>, 2014.](#)

- Döll, P., Hoffmann-Dobrev, H., Portmann, F. T., Siebert, S., Eicker, A., Rodell, M., Strassberg, G., and Scanlon, B. R.: Impact of water withdrawals from groundwater and surface water on continental water storage variations, *Journal of Geodynamics*, 59-60, 143–156, <https://doi.org/10.1016/j.jog.2011.05.001>, 2012.
- 690 Döll, P., Kaspar, F., and Lehner, B.: A global hydrological model for deriving water availability indicators: model tuning and validation, *Journal of Hydrology*, 270, 105–134, [https://doi.org/10.1016/S0022-1694\(02\)00283-4](https://doi.org/10.1016/S0022-1694(02)00283-4), 2003.
- Flörke, M., Kynast, E., Bärlund, I., Eisner, S., Wimmer, F., and Alcamo, J.: Domestic and industrial water uses of the past 60 years as a mirror of socio-economic development: A global simulation study, *Global Environmental Change*, 23, 144–156, <https://doi.org/10.1016/j.gloenvcha.2012.10.018>, 2013.
- 695 Heim, R. R.: A review of twentieth-century drought indices used in the United States, *Bull. Amer. Meteor. Soc.*, 83, 1149–1166, <https://doi.org/10.1175/1520-0477-83.8.1149>, 2002.
- Hogg, E. H., Barr, A. G., and Black, T. A.: A simple soil moisture index for representing multi-year drought impacts on aspen productivity in the western Canadian interior, *Agricultural and Forest Meteorology*, 178-179, 173–182, <https://doi.org/10.1016/j.agrformet.2013.04.025>, 2013.
- 700 Hosseini-Moghari, S.-M., Araghinejad, S., Tourian, M. J., Ebrahimi, K., and Döll, P.: Quantifying the impacts of human water use and climate variations on recent drying of Lake Urmia basin: the value of different sets of spaceborne and in situ data for calibrating a global hydrological model, *Hydrol. Earth Syst. Sci.*, 24, 1939–1956, <https://doi.org/10.5194/hess-24-1939-2020>, 2020.
- Hunger, M. and Döll, P.: Value of river discharge data for global-scale hydrological modeling, *Hydrol. Earth Syst. Sci.*, 12, 841–861, <https://doi.org/10.5194/hess-12-841-2008>, 2008.
- 705 Kumar, N., Murthy, S., Sai, S., and Roy, S.: On the use of Standardized Precipitation Index (SPI) for drought intensity assessment, Meteorological applications, <https://doi.org/10.1002/met.136>, available at: <http://arxiv.org/pdf/1509.04808v1>, 2009.
- Langat, P. K., Kumar, L., and Koech, R.: Identification of the Most Suitable Probability Distribution Models for Maximum, Minimum, and Mean Streamflow, *Water*, 11, 734, <https://doi.org/10.3390/w11040734>, 2019.
- 710 López-Moreno, J. I., Vicente-Serrano, S. M., Beguería, S., García-Ruiz, J. M., Portela, M. M., and Almeida, A. B.: Dam effects on droughts magnitude and duration in a transboundary basin: The Lower River Tagus, Spain and Portugal, *Water Resour. Res.*, 45, 6, <https://doi.org/10.1029/2008WR007198>, 2009.
- Lorenzo-Lacruz, J., Vicente-Serrano, S. M., López-Moreno, J. I., Beguería, S., García-Ruiz, J. M., and Cuadrat, J. M.: The impact of droughts and water management on various hydrological systems in the headwaters of the Tagus River (central Spain), *Journal of Hydrology*, 386, 13–26, <https://doi.org/10.1016/j.jhydrol.2010.01.001>, 2010.
- 715 Mckee, T. B., Doesken, N. J., and Kleist, J.: The relationship of drought frequency and duration times scales, *Eight conference on Applied Climatology*, 17–22, 1993.

- 720 [Meza, I., Siebert, S., Döll, P., Kusche, J., Herbert, C., Eyshi Rezaei, E., Nouri, H., Gerdener, H., Popat, E., Frischen, J., Naumann, G., Vogt, J., Walz, Y., Sebesvari, Z., and Hagenlocher, M.: Global-scale drought risk assessment for agricultural systems, *Nat. Hazards Earth Syst. Sci.*, 20, 695–712, <https://doi.org/10.5194/nhess-20-695-2020>, 2020.](#)
- [Modarres, R.: Streamflow drought time series forecasting, *Stoch Environ Res Ris Assess.*, 21, 223–233, <https://doi.org/10.1007/s00477-006-0058-1>, 2007.](#)
- 725 [Müller Schmied, H., Cáceres, D., Eisner, S., Flörke, M., Niemann, C., Peiris, T. A., Popat, E., Portmann, F. T., Reinecke, R., Schumacher, M., Shadkam, S., Telteu, C. E., Trautmann, T., and Döll, P.: The global water resources and use model WaterGAP v2.2d: Model description and evaluation, submitted to *Geoscientific Model Development*, 2020.](#)
- [Müller Schmied, H., Eisner, S., Franz, D., Wattenbach, M., Portmann, F. T., Flörke, M., and Döll, P.: Sensitivity of simulated global-scale freshwater fluxes and storages to input data, hydrological model structure, human water use and calibration, *Hydrol. Earth Syst. Sci.*, 18, 3511–3538, <https://doi.org/10.5194/hess-18-3511-2014>, 2014.](#)
- 730 [Neena, J. M., Suhas, E., and Goswami, B. N.: Leading role of internal dynamics in the 2009 Indian summer monsoon drought, *J. Geophys. Res.*, 116, <https://doi.org/10.1029/2010JD015328>, 2011.](#)
- [Palmer, W. C.: Meteorological drought, 45, Washington, D.C., 58, 1965.](#)
- [Richter, B. D., Davis, M. M., Apse, C., and Konrad, C.: A presumptive standard for environmental flow protection, *River Res. Applic.*, 28, 1312–1321, <https://doi.org/10.1002/rra.1511>, 2012.](#)
- 735 [Seager, R.: The Turn of the Century North American Drought: Global Context, Dynamics, and Past Analogs*, *J. Climate*, 20, 5527–5552, <https://doi.org/10.1175/2007JCLI1529.1>, 2007.](#)
- [Sharma, T. C. and Panu, U. S.: Predicting return periods of hydrological droughts using the Pearson 3 distribution: a case from rivers in the Canadian prairies, *Hydrological Sciences Journal*, 60, 1783–1796, <https://doi.org/10.1080/02626667.2014.934824>, 2015.](#)
- 740 [Sheffield, J., Goteti, G., Wen, F., and Wood, E. F.: A simulated soil moisture based drought analysis for the United States, *J. Geophys. Res.*, 109, 7449, <https://doi.org/10.1029/2004JD005182>, 2004.](#)
- [Siebert, S., Kumm, M., Porkka, M., Döll, P., Ramankutty, N., and Scanlon, B.: Historical Irrigation Dataset \(HID\), 2015.](#)
- [Spinoni, J., Barbosa, P., Jager, A. de, McCormick, N., Naumann, G., Vogt, J. V., Magni, D., Masante, D., and Mazzeschi, M.: A new global database of meteorological drought events from 1951 to 2016, *Journal of Hydrology: Regional Studies*, 22, 100593, <https://doi.org/10.1016/j.ejrh.2019.100593>, 2019.](#)
- 745 [Sridhar, V., Hubbard, K. G., You, J., and Hunt, E. D.: Development of the soil moisture index to quantify agricultural drought and Its “user friendliness” in severity-area-duration assessment, *J. Hydrometeorol.*, 9, 660–676, <https://doi.org/10.1175/2007JHM892.1>, 2008.](#)
- 750 [Svensson, C., Hannaford, J., and Prosdocimi, I.: Statistical distributions for monthly aggregations of precipitation and streamflow in drought indicator applications, *Water Resour. Res.*, 53, 999–1018, <https://doi.org/10.1002/2016WR019276>, 2017.](#)

van Loon, A. F.: On the propagation of drought: How climate and catchment characteristics influence hydrological drought development and recovery, s.n.l. IS.I., 196 pp., 2013.

755 van Loon, A. F., Stahl, K., Di Baldassarre, G., Clark, J., Rangelcroft, S., Wanders, N., Gleeson, T., van Dijk, A. I. J. M., Tallaksen, L. M., Hannaford, J., Uijlenhoet, R., Teuling, A. J., Hannah, D. M., Sheffield, J., Svoboda, M., Verbeiren, B., Wagener, T., and Van lanen, H. A. J.: Drought in a human-modified world: reframing drought definitions, understanding, and analysis approaches, *Hydrol. Earth Syst. Sci.*, 20, 3631–3650, <https://doi.org/10.5194/hess-20-3631-2016>, 2016.

760 Veldkamp, T. I. E., Zhao, F., Ward, P. J., Moel, H. de, Aerts, J. C. J. H., Schmied, H. M., Portmann, F. T., Masaki, Y., Pokhrel, Y., Liu, X., Satoh, Y., Gerten, D., Gosling, S. N., Zaherpour, J., and Wada, Y.: Human impact parameterizations in global hydrological models improve estimates of monthly discharges and hydrological extremes: a multi-model validation study, *Environ. Res. Lett.*, 13, 55008, <https://doi.org/10.1088/1748-9326/aab96f>, 2018.

Vicente-Serrano, S. M., Beguería, S., and López-Moreno, J. I.: A Multiscalar Drought Index Sensitive to Global Warming: The Standardized Precipitation Evapotranspiration Index, *J. Climate*, 23, 1696–1718, <https://doi.org/10.1175/2009JCLI2909.1>, 2010.

765 Wu, H., Hayes, M. J., Weiss, A., and Hu, Q.: An evaluation of the Standardized Precipitation Index, the China-Z Index and the statistical Z-Score, *Int. J. Climatol.*, 21, 745–758, <https://doi.org/10.1002/joc.658>, 2001.

770 Zaherpour, J., Mount, N., Gosling, S. N., Dankers, R., Eisner, S., Gerten, D., Liu, X., Masaki, Y., Müller Schmied, H., Tang, Q., and Wada, Y.: Exploring the value of machine learning for weighted multi-model combination of an ensemble of global hydrological models, *Environmental Modelling & Software*, 114, 112–128, <https://doi.org/10.1016/j.envsoft.2019.01.003>, available at: <http://www.sciencedirect.com/science/article/pii/S1364815217309817>, 2019.

775 Zaherpour, J., Gosling, S. N., Mount, N., Schmied, H. M., Veldkamp, T. I. E., Dankers, R., Eisner, S., Gerten, D., Gudmundsson, L., Haddeland, I., Hanasaki, N., Kim, H., Leng, G., Liu, J., Masaki, Y., Oki, T., Pokhrel, Y., Satoh, Y., Schewe, J., and Wada, Y.: Worldwide evaluation of mean and extreme runoff from six global-scale hydrological models that account for human impacts, *Environ. Res. Lett.*, 13, 65015, <https://doi.org/10.1088/1748-9326/aac547>, 2018.